Research in Health Science
ISSN 2470-6205 (Print) ISSN 2470-6213 (Online)
Vol. 10, No. 3, 2025
www.scholink.org/ojs/index.php/rhs

Original Paper

Integrative Bioinformatics Identification of Hub Genes in Renal Ischemia-reperfusion Injury: A Multi-dataset Consensus Approach Combining Conventional and Dietary Restriction Models

Simin Li[1*]

[1] Stomatological Hospital, School of Stomatology, Southern Medical University, 366 Jiangnan South Avenue, Haizhu district, Guangzhou 510280, Guangdong province, China

[*] Corresponding author: simin.li.dentist@gmail.com

Received: January 5, 2025 Accepted: June 7, 2025 Online Published: June 12, 2025

doi:10.22158/rhs.v10n3p1 URL: http://dx.doi.org/10.22158/rhs.v10n3p1

Abstract

Background: *Ischemia reperfusion injury (IRI) involves the cellular damage, dysfunction and cell death subsequent to the reperfusion of previously ischemic tissues. The molecular mechanisms of IRI are not well understood.* ***Methods:*** *We used an integrative bioinformatic analysis to identify key molecular mechanisms involved in IRI by utilizing 7 publically available gene expression datasets from conventional and dietary restriction related IRI. Differential gene expression (DEG) analysis and functional enrichment analysis was performed. Hub IRI related genes were identified using a consensus approach from 4 methods; weighted gene co-expression network analysis, immune infiltration analysis, ANOVA with LASSO regression and cluster analysis. Receiver operating curve analysis and support vector machine analysis were performed to examine prediction accuracy. Differential expression analysis of a miRNA-related dataset was performed and a hub gene-DEmiRNA-lncRNA network analysis was constructed.* ***Results:*** *34 IRI-related genes were identified. Enriched functions included cellular hormone metabolic process and progesterone metabolic process, regulation of Protein digestion and absorption, 2-Oxocarboxylic acid metabolism and AGE-RAGE signaling pathway. Five consensus hub IRI related hub genes; Hpd, Cyp2d9, Aldh1a2, Pigr, Bcat1 were obtained. ROC and SVM analysis indicated high AUC values for the IRI related hub genes. Cyp2d9 was highly correlated with Hpd and Pigr. Hub gene-DEmiRNA-lncRNA network analysis showed Bcat1 as regulated by multiple DEmiRNAs.* ***Conclusion:*** *Using an integrated bioinformatics analysis approach the molecular mechanisms of IRI were deconstructed and 5 candidate genes very highly relevant to IRI pathogenesis were identified. These findings present valuable directions for future translational research.*

Keywords

Ischemia-reperfusion injury, Gene expression profiling, Hub genes, Biomarkers, Kidney transplantation

1. Introduction

Ischemia occurs due to hypoperfusion, when blood supply to a tissue or organ is interrupted causing a drastic reduction in the oxygen and glucose, which leads to metabolic derangement and tissue injury (Wu et al., 2018). ATP levels and pH decline in this phase due to anaerobic metabolism (Kalogeris et al., 2012). Tissue injury occurs during the reperfusion occurs due to an increase in molecular oxygen which leads to the activation of several downstream pathways including the xanthine oxidase system, neutrophil activation, mitochondrial electron transport chain, arachidonic acid metabolism and oxidation of catecholamines (Wu et al., 2018). These result in the production of several reactive oxygen species (ROS) that result in ischemia reperfusion injury (IRI) via modulating the mitochondrial permeability transition pore (Bains, 2009). Consequently, a cascade of complex pathological processes including membrane lipid peroxidation, complement activation, proinflammatory cytokines, and endothelial activation are triggered, mediating IRI.

Clinically, IRI can cause critical organ damage and may occur after multiple conditions that lead to hypoperfusion including sepsis, organ transplant, trauma, stroke or myocardial infarction. Renal IRI is a chief cause of acute kidney injury and failure in humans, which is associated with high mortality rates. In case of renal transplantation, IRI can occur frequently, especially in cases of allograft organ transplant, which can lead to delayed graft function and affect graft survival. Emerging management modalities include the renal delivery of pharmacological agents during machine perfusion (Franzin et al., 2021). The identification of novel targets to manage renal IRI requires an unraveling of complex molecular mechanisms implicated in its pathogenesis

Dietary and protein restriction can mitigate renal IRI by inducing metabolic alterations (Jongbloed et al., 2014; Jongbloed et al., 2017). Several studies have analyzed molecular underpinnings of renal IRI using bioinformatics (Feng et al., 2016; Zhu eta l., 2018; Guo et al., 2019; You et al., 2022) but integrative analyses based on multiple datasets from IRI under conventional and dietary restriction conditions are lacking. Such integrative analysis can aid a deeper understanding of key molecular mechanisms underpinning renal IRI. Here, we aimed to perform integrative analysis of multiple datasets related to conventional and dietary restriction related ischemia-reperfusion injury experiments to obtain high relevance genes that might play crucial roles in ischemia-reperfusion injury.

2. Material and Method

2.1 Datasets

We downloaded datasets related to ischemia-reperfusion injury (IRI) from GEO (http://www.ncbi.nlm.nih.gov/) and obtained a total of 7 datasets (Table 1). These include 6

mouse-related datasets: (GSE98622, GSE29495, GSE39548, GSE65656, GSE52982, GSE182793), and one human-related dataset (GSE142077). GSE98622 pertains to ischemia-reperfusion injury in kidney tissue, and GSE65656 and GSE52982 were from tissue ischemia-reperfusion injury under dietary restrictions.

Table 1. IRI Datasets

Accession	Platforms	Series Type	Taxonomy	Sample Count	Sample Characteristics
GSE98622	GPL13112 GPL19057	Expression profiling by high throughput sequencing	Mouse	49	Normal(Control), Sham, IRI
GSE29495	GPL13642	Non-coding RNA profiling by array	Mouse	16	Sham, IRI
GSE39548	GPL7202	Expression profiling by array	Mouse	20	Control, IRI, IRI+Hemin, IPC+IRI, Hemin
GSE65656	GPL11180	Expression profiling by array	Mouse	36	Control (SDS), 3 days fasting, 2 weeks 30% dietary restriction, Control (type I), 3 days protein-free, 3 days fat-free, 3 days carbohydrate-free
GSE52982	GPL11180	Expression profiling by array	Mouse	19	Young-control, Young-fasted, Old-control, Old-fasted
GSE182793	GPL21103	Expression profiling by high throughput sequencing	Mouse	12	Control, IRI conscious, IRI anesthesia
GSE142077	GPL16791	Expression profiling by high throughput sequencing	Human	15	Normal(Control), Ischemia, Reperfusion

In the 6 mouse-related datasets, GSE98622 and GSE182793 included expression profiling by high throughput sequencing, GSE29495 included non-coding RNA profiling by array, and the GSE39548, GSE65656, and GSE52982 included gene expression profiling by array. The human-related dataset GSE142077 included expression profiling by high throughput sequencing. We performed statistical analysis on the datasets grouped into different experimental types. We mainly analyzed GSE98622, GSE65656 and GSE52982, and other datasets were used to validate the analysis results.

2.2 Data Preprocessing

After downloading the data, we first converted the Probe IDs in the expression matrix to Gene Symbol according to the platform information. If one Probe ID matched multiple Gene Symbols, then we deduplicated the Gene Symbol by the average of the sample expression values. After performing the Gene Symbol conversion, if the sample expression value was large, we considered log2 for the expression value of the sample. For a dataset of experimental type expression profiling by high throughput sequencing, if the expression value type was Count, we converted count to a TPM (Transcripts per million) value based on Equation 1. If the number of samples with a gene expression value of 0 in the expression matrix exceeded half of the total number of samples, we removed the gene from the expression matrix.

$$\mathrm{TPM} = \frac{Ni / Li * 10^6}{sum(N1/L1 + N2/L2 + ... + Nn/Ln)} \quad \text{(Equation 1)}$$

Ni is the read counts that mapped on the exon i. Li is the length of exon i. $sum(N1/L1 + N2/L2 + ... + Nn/Ln)$ is the sum of all exons normalized by length.

Since experimental types of GSE65656 and GSE52982 were gene expression profiling by array, we combined the two expression matrices together for analysis and used the ComBat method in the SVA package of R (version 4.1.3) to eliminate the batch effects while merging data. We performed PCA analysis on the expression matrices before and after the merge to analyze the effects of the merge. We labeled the merged data as GSE52982 & GSE65656.

2.3 Differential Expression Analysis

Differential expression analysis is the comparison of expression values of different groups of samples in a dataset, through which it is possible to detect whether genes have differences between different sample groups. For GSE98622, we first performed differential expression analysis based on Case-sample vs Normal-sample, and then differential expression analysis based on Case-sample vs Sham-sample. For GSE52982 & GSE65656, we distinguished between samples based on whether dietary restrictions were enforced, defining dietary restriction-related samples as Case-samples, non-dietary restriction-related samples as Control-samples, and differential expression analysis based on Case-sample vs Control-sample.

We used the "limma" package of R to analyze the differential expression of GSE98622, GSE52982 &GSE65656. We defined the thresholds of P.adjust and log2FC (log2 fold change) based on the analysis results, so as to obtain differentially expressed genes (DEG). For GSE98622, the genes with

P.adjust<0.05 and | log2FC|>1 were selected as the DEGs. For GSE52982 &GSE65656, the genes with P.adjust < 0.05 and the |log2FC |> 0.5 were considered DEGs.

2.4 Screening of IRI Related Genes

First, we obtained the DEGs with the similar expression trend in the differential expression analysis results of the GSE98622 dataset (Case-sample vs Normal-sample, Case-sample vs Sham-sample). These genes were not affected by sham. We then intersected these DEGs obtained from the GSE98622 dataset and GSE52982 & GSE65656, which were labeled IRI related genes. These IRI related genes differed not only in the level of expression in conventional ischemic reperfusion experiments, but also in the level of expression in ischemic reperfusion experiments under food restriction.

2.5 Enrichment Analysis of IRI Related Genes

We used the “clusterProfiler " package in R to analyze the IRI related gene for enriched GO Biological process and KEGG pathways. We selected pvalue < 0.05 as the significance threshold to determine biological processes affected by these IRI related genes.

2.6 Prediction of Hub IRI Related Genes

We analyzed the IRI datasets from different perspectives using 4 different methods to predict hub IRI related genes.

2.6.1 Method 1: Global Analysis of IRI Using Weighted Gene Co-Expression Network Analysis (WGCNA)

If genes have similar expression changes in a physiological process or in different tissues, then these genes are also potentially functionally related. In this method, a module is defined as a group of genes with a similar expression profile. We used the “WGCNA” package in R (Langfelder et al., 2008) to analyze GSE98622, GSE52982 & GSE65656, respectively. We first obtained the expression matrix of all genes in case samples under 2 datasets, and then established a co-expression network of genes and samples. A co-expression network is a scale-free weighted network. In order to meet the preconditions for a scaleless network distribution as much as possible, we selected the value of the adjacency matrix weight parameter β. We set the β values to 1-30 and calculated the correlation coefficients and gene adjacency functions for the two IRI datasets. Among these, the higher the correlation coefficient (R^2) (maximum is 1), the closer the network was to the network-free scale distribution, but at the same time a certain degree of gene connectivity needs to be guaranteed, so this β value should be as small as possible while the correlation coefficient is large enough.

After selecting the β value, we used the ‘TOMsimilarity’ method to establish the given adjacency matrix according to the expression matrix, and then used ‘cutreeDynamic’ to cut the given adjacency matrix, so as to achieve module mining of the dataset. After obtaining the modules, we used the ‘mergeCloseModules’ method to merge the modules with correlation coefficients greater than 0.8 and determine the corresponding sample fractions of the modules based on the gene expression values in the modules. We extracted the modules in which DEGs were located in the two datasets, and then scored the module significance according to the P.adj value corresponding to the DEGs in the differential expression

analysis, and finally determined the relatively significant modules in the dataset based on the mean (P.adj) score. We extracted the IRI related genes in the significant modules, analyzed the Pearson correlation coefficient between the corresponding sample fraction of the module and the expression value of the IRI related gene samples, and assessed the relationship between the different modules and the IRI related genes. We finally intersected the IRI related genes in the GSE98622, GSE52982 & GSE65656 significant modules to obtain the hub genes determined by WGCNA.

2.6.2 Method 2: Immune Infiltration Analysis with ESTIMATE

We obtained the expression values of DEGs in GSE98622, GSE52982 & GSE65656, respectively, and used the "biomaRt" package of R for homologous comparison of mouse and human genes. Using homologous comparison, we replaced mouse genes in the two sets of expression matrices with human genes. When a human gene corresponds to multiple mouse genes, to ensure gene uniqueness, we de-weight the expression matrix by mean.

We used the ESTIMATE algorithm (Yoshihara et al., 2013) to calculate two sets of expression matrices separately to obtain stromal cell fractions and immune cell fractions in IRI-related kidney tissue samples. We used the Wilcoxon test to analyze the differences of immune cells in the case and control groups. At the same time we performed ROC analysis of the cell fractions in the sample to assess the robustness of ESTIMATE. Then we extracted the results of immune cells and IRI related genes in the case samples, and analyzed the relationship between the stromal cell samples and the IRI related genes using Pearson correlation coefficient, and analyzed the relationship between the immune cell samples and the IRI related genes. Finally, we filtered for IRI related genes. For GSE98622, GSE52982 & GSE65656, we extracted a gene if it was relatively highly correlated with both dataset stromal cells. Similarly, if a gene was relatively highly correlated with both datasets of immune cells, we extracted it. Finally, we took the IRI related genes that were highly correlated with stromal cells and immune cells to obtain hub genes associated with ESTIMATE.

2.6.3 Method 3: IRI Related Genes Analyzed Using ANOVA and LASSO

We extracted the expression values of IRI related genes in GSE98622, GSE52982 & GSE65656, and then performed ANOVA analysis of the IRI related genes in the datasets based on sample type (Case and Control). We obtained IRI related genes (Pvalue<0.01) that were significant in both datasets, and then used LASSO (Least absolute shrinkage and selection operator) Logistic Regression (Tibshirani, 1996) to characterize the significant IRI related genes. We used LASSO to build models for feature screening in two sets of datasets (GSE98622, GSE52982 & GSE65656), and finally obtained IRI-related hub genes.

2.6.4 Method 4: Consensus Cluster Plus to Analyze Case-samples Corresponding to IRI Related Genes

We obtained the expression matrix of IRI related genes in Case-samples in GSE98622, GSE52982 & GSE65656, and then analyzed it using "ConsensusClusterPlus" in R.To obtain samples with consistent correlation, we set the maxK parameter to 8 in the ConsensusClusterPlus method, and then selected the best Cluster from the clustering results. Based on the samples in different Clusters, we used "limma" in R to perform multi-group differential expression analysis on IRI related genes in GSE98622, GSE52982, &

GSE65656. We combined IRI related genes from 2 datasets of P value < 0.05 to obtain the hub genes associated with ConsensusClusterPlus. We used a boxplot to depict these hub gene expressions in different Clusters samples and performed kruskal.test to determine significance.

We analyzed IRI through the above 4 methods to obtain 4 different sets of hub genes. If a gene appeared in any of the 3 methods, then this gene was considered a potential hub gene in IRI, and these potential hub genes were included in subsequent analyses.

2.7 ROC Analysis for Hub IRI Related Genes

We extracted the expression values of the hub IRI related gene in GSE98622, GSE52982 & GSE65656 and then performed the Wilcoxon Test. We simultaneously extracted the expression values of hub IRI related genes in three validation sets (GSE29495, GSE39548, GSE182793) to see the differences between these genes in the validation set. Finally, we performed a ROC analysis of hub IRI related genes to assess the prediction strength of the expression levels of these genes.

2.8 SVM Analysis of Hub IRI Related Genes

We build SVM models based on Case-samples and Control-samples, using each hub IRI related gene as a feature to evaluate the model's predictive effect through ROC analysis. We used Python's scikit-learn package to build the SVM model. After establishing the SVM, we examined the SVM using the GridSearchCV method and used 10 fold cross-validation to find the best parameters. We divided the dataset into training sets and test sets at 70%/30%, the training set was used for model identification of data features, and the test set was used to verify the learning effect of the model. The score of each sample was obtained using the model prediction, and we used the sample score to perform ROC analysis to evaluate the effectiveness of the model.

For IRI-related datasets, we obtained the expression matrix of hub IRI related gene in each dataset and performed the following 3-step processing:

① S1: Based on hub genes, GSE98622, GSE52982&GSE65656 expression matrices were merged. The samples were divided into training sets and test sets at 70%/30%. The prediction effect was evaluated after the SVM was established

② S2: Based on hub genes, GSE39548, GSE182793, GSE142077 expression matrices were merged. Hub genes that appeared in 3 datasets were used for combining, and then we divided the samples into training sets and test sets at 70%/30%. Next, we built the SVM model and evaluated the prediction values.

③ S3: Based on hub genes, we merged five sets of data expression matrices (a total of 6 datasets) in steps S1 and S2. During the merging process, we merged hub genes that appeared together in 3 datasets. The samples were divided into training sets and test sets at 70%/30%. The prediction values were evaluated after the SVM was established.

Next, we used the Pearson correlation coefficient to analyze the correlations between the hub genes.

2.9 Differential Expression Analysis of GSE29495 and Construction of ceRNA Network

Differential expression analysis of the miRNA-related dataset GSE29495 was performed to screen for

differentially expressed miRNA (DE-miRNA). We predicted miRNAs targeting hub genes through the miRWalk database (http://mirwalk.umm.uni-heidelberg.de/). These miRNAs were then intersected with DEmiRNAs, and finally the DEmiRNA-hub gene pairs were obtained.

We downloaded the relationship pairs of miRNA and lncRNA from the ENCORI database (https://starbase.sysu.edu.cn/index.php) and extracted the de-miRNA corresponding lncRNA targets to form DEEmiRNA-lncRNA relationship pairs. Integrating hub gene-DEmiRNA, DEmiRNA-lncRNA was done using Cytoscape software to construct ceRNA networks. Pearson's correlation coefficient was used to analyze the relationship between miRNAs in ceRNA networks.

3. Results

3.1 Data Preprocessing

We first combined GSE65656 and GSE52982 directly for PCA analysis (Fig1A). The results showed that some of the samples between GSE65656 and GSE52982 were coincident. (a region of Fig1A). By comparing the raw data, we identified these samples from the same group of mice. Therefore, we did not process samples from *a* region. For samples in the b region , we used the “ComBat” method of “sva” packages of R to eliminate batch effects (Fig1B). By comparing the b-region samples in Fig1A and Fig1B, it was found that the difference in the b-region in Fig1B was significantly reduced, and all samples from the a and b regions in Fig1B were integrated for subsequent analysis.

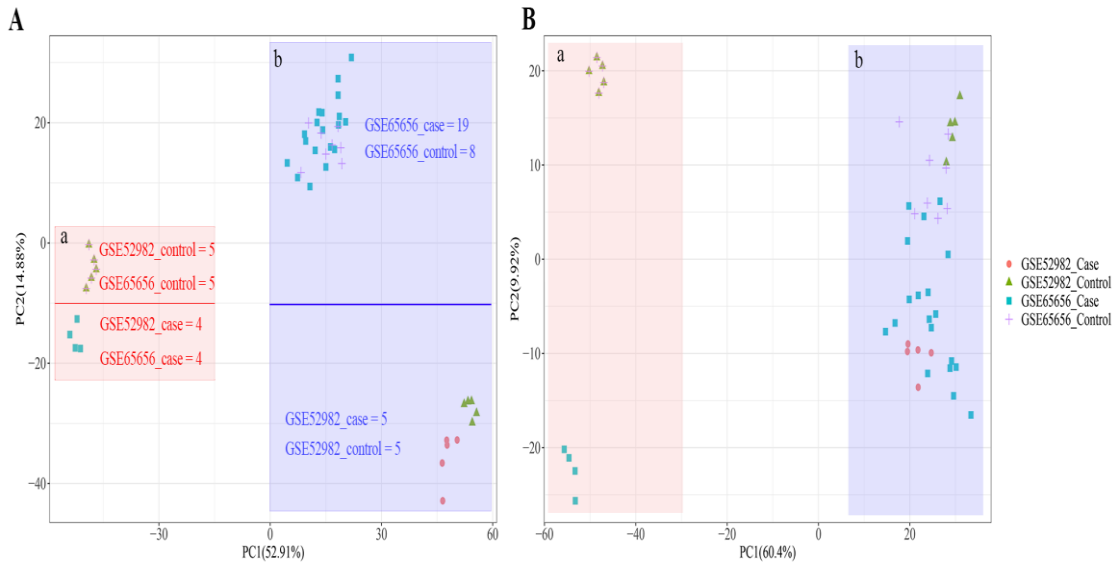

Figure 1. PCA Analysis of Dataset Merging and Batch Effect Correction. (A) PCA analysis of GSE65656 and GSE52982 before batch effect correction. (B) PCA analysis after eliminating batch effects using the ComBat method. In the figure, samples in area a are from the same group, and samples in area b are from different groups. Batch effects were eliminated only for samples in area b, and finally samples in areas a and b were merged for subsequent analysis.

3.2 Differential Expression Analysis

We performed differential expression analysis on GSE98622, GSE52982 & GSE65656. For GSE98622, we selected genes with P.adjust<0.05 and |log2FC|>1 as differentially expressed genes, where log2FC>1 was up-regulated and log2FC <-1 was down-regulated (Table 2). For GSE52982&GSE65656, we selected genes with P.adjust<0.05 and |log2FC|>0.5 as differentially expressed genes (DEGs). Here, genes with log2FC>0.5 were up-regulated genes, and those with log2FC<0.5 were down-regulated genes (Table 2). We used a volcano plot to depict the distribution of differential expressed genes between the two datasets, and marked the Top 10 genes with the most significant P.adjust values on the plot (Fig. 2).

Table 2. DEG Statistical Results

	GSE98622		**GSE52982&GSE65656**
	Case vs Normal	**Case vs Sham**	**Case vs Control**
P.adjust	P.adjust < 0.05		
|log2FC|	|log2FC| > 1		|log2FC| > 0.5
DEG_up	293	564	135
DEG_down	150	106	358
DEG_total	443	670	493

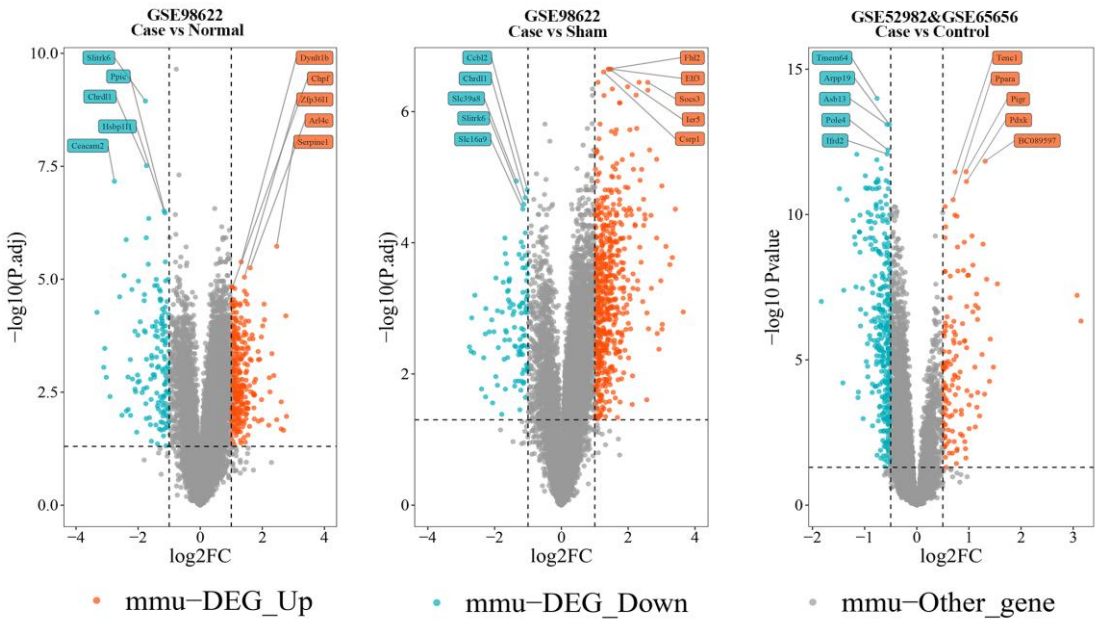

Figure 2. Volcano Plot of Differentially Expressed Genes Distribution in GSE98622, GSE52982 & GSE65656. The plots show the distribution of differentially expressed genes with the top 10 genes with the most significant P.adjust values marked. Red dots represent upregulated genes, blue dots represent downregulated genes, and gray dots represent genes that do not meet the significance criteria.

3.3 Screening for IRI Related Genes

After differential expression analysis, we obtained a total of 269 DEGs for GSE98622 (case vs normal, case vs sham) (Figure 3A). Among these, there were 268 genes with the same expression trend, including 200 commonly up-regulated genes and 68 common genes that were down-regulated.

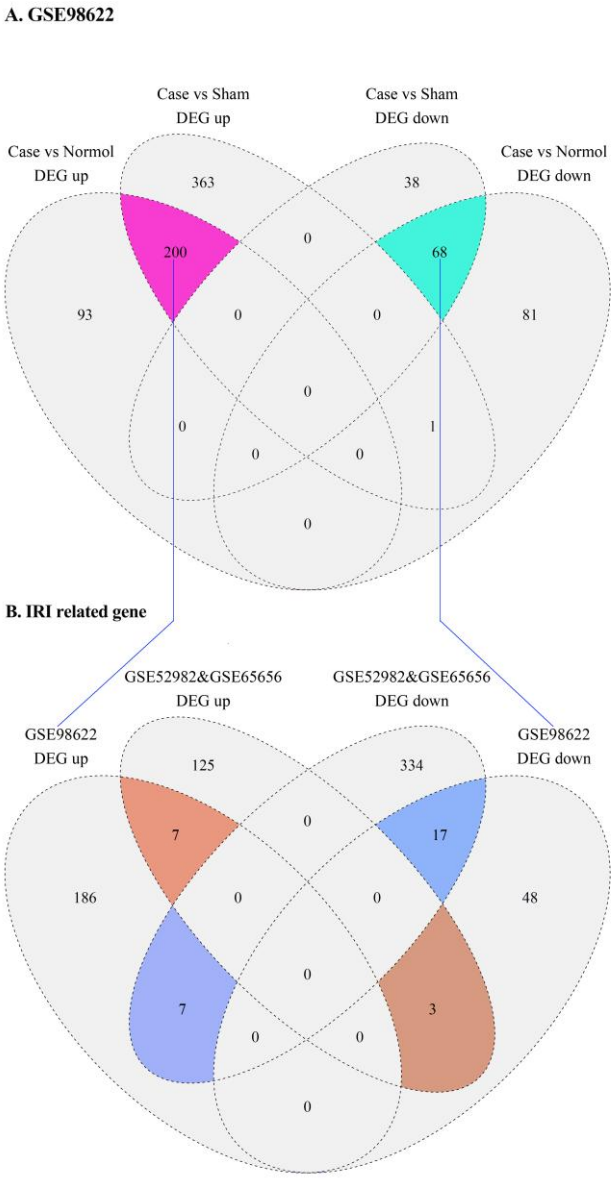

Figure 3. IRI Related Gene Venn Diagram from DEG. (A) Differentially expressed genes obtained from GSE98622 dataset showing overlap between Case vs Normal and Case vs Sham comparisons. (B) IRI related genes obtained from the intersection of GSE98622 and GSE52982&GSE65656 datasets, resulting in 34 IRI-related genes.

We extracted the expression values of IRI related genes in GSE98622, GSE52982&GSE65656, and obtained the dataset-related characteristics. The results indicated that the expression levels of IRI related genes in case and control samples were significantly different (Figure 4A-B).

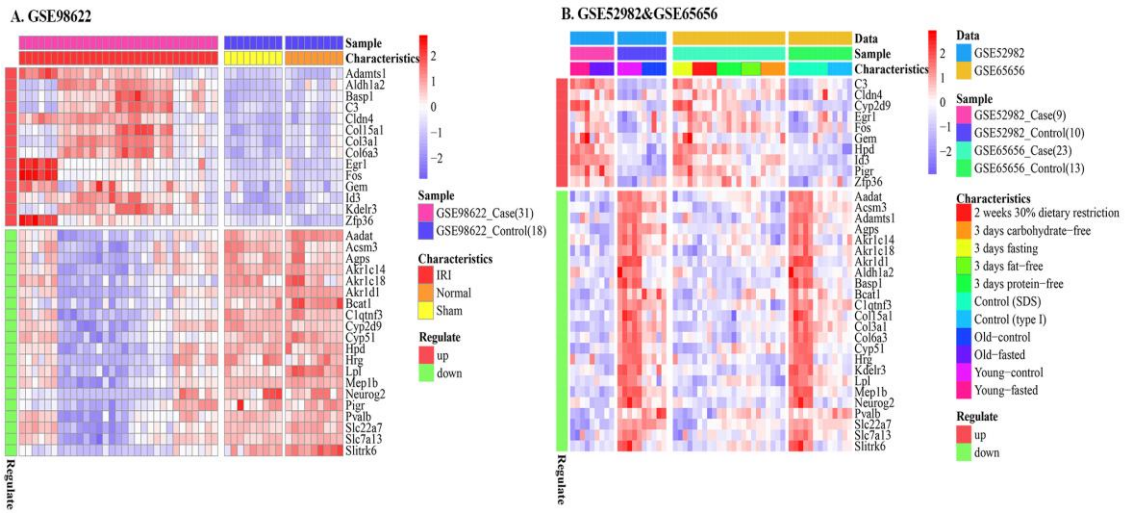

Figure 4. Expression Values of IRI Related Genes in GSE98622 and GSE52982&GSE65656. Heatmaps showing the expression patterns of 34 IRI-related genes across different sample conditions. Red indicates high expression, blue indicates low expression. Sample characteristics are color-coded and shown on the top.

In order to obtain the expression levels of 34 IRI related genes under different treatment conditions in GSE39548, GSE182793 and GSE142077, we obtained the expression matrices of these genes in three datasets. Since GSE142077 is a human data expression matrix, we used the “biomaRt” package of R to perform homologous alignment of mouse and human genes to find the corresponding human genes. Finally, we obtained 32 human-related genes. The expression matrix of IRI related genes in GSE142077 was obtained using 32 human genes, and the three groups of expression matrices were displayed by heat map (Figure 5A-C).

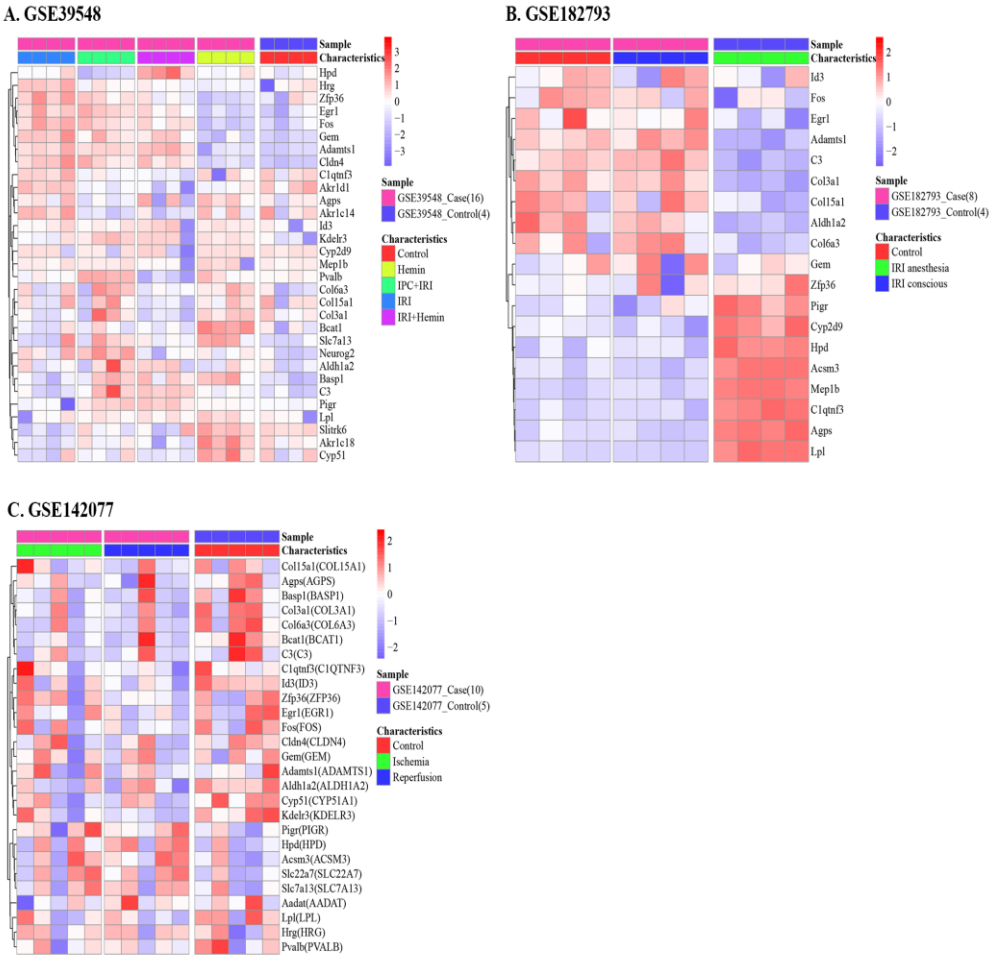

Figure 5. Heat Map of Expression Levels of IRI Related Genes in Validation Datasets. (A) GSE39548, (B) GSE182793 and (C) GSE142077. Since data cleaning was performed for each dataset, the number of IRI related genes obtained in GSE39548, GSE182793 and GSE142077 were 31, 19 and 27, respectively. In Figure 5C, the human genes are in brackets, and the mouse genes are outside the brackets.

We used the “clusterProfiler" package of R to perform GO Biological process and KEGG pathway analysis on these 34 mouse-related IRI related genes, and selected Pvalue<0.05 as the significant pathway and displayed the Top20 pathway (Figure 6AB). At the same time, we performed GO Biological process and KEGG pathway analysis on 32 human-related IRI related genes, selected Pvalue<0.05 as the significant pathway and displayed the Top20 pathway (Figure 6 C-D). The results showed that mouse and human IRI related genes are mainly involved in biological processes such as cellular hormone metabolic process and progesterone metabolic process (Figure 6A, Figure 6C); regulate Protein digestion and absorption, 2-Oxocarboxylic acid metabolism, AGE-RAGE signaling pathway in diabetes complications and other pathways (Figure 6B, Figure 6D).

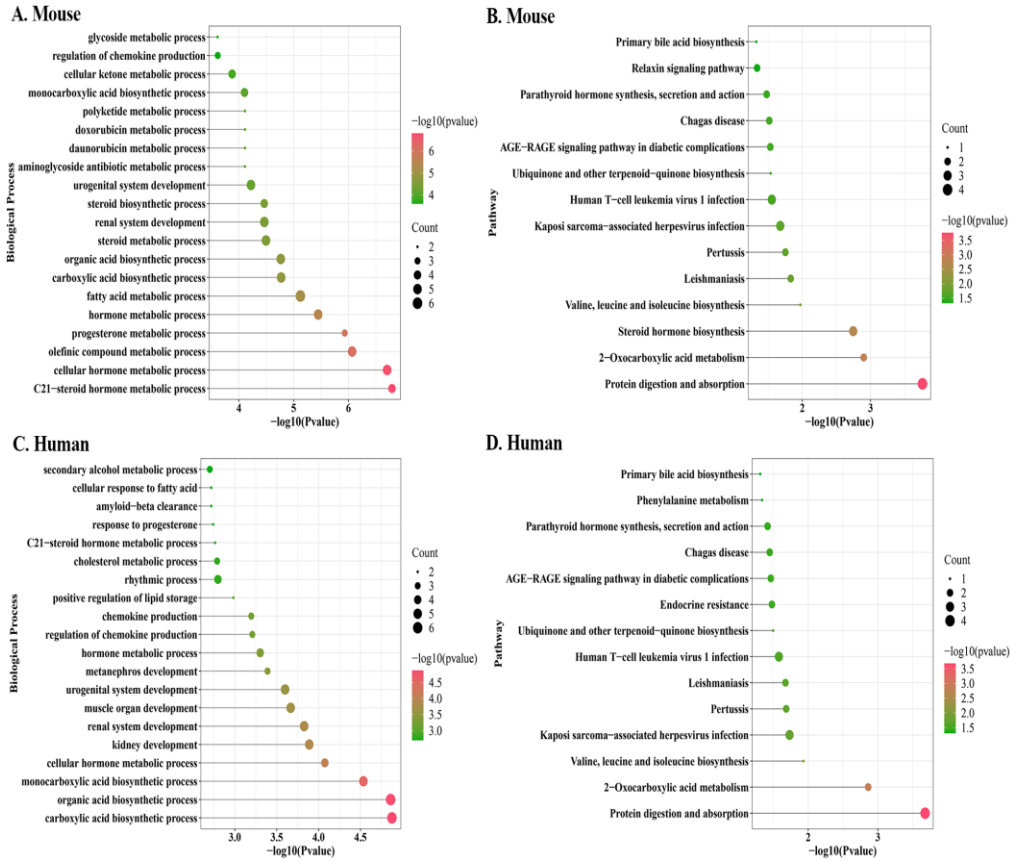

Figure 6. Biological Processes and Pathways Significantly Regulated by IRI Related Genes. (A-B) Biological processes and pathways significantly regulated by mouse IRI related genes; (C-D) Biological processes and pathways significantly regulated by human IRI related genes. The results show enrichment in cellular hormone metabolic processes, progesterone metabolic processes, protein digestion and absorption, 2-Oxocarboxylic acid metabolism, and AGE-RAGE signaling pathway.

3.4 Screening Hub IRI Related Genes

We further screened 34 IRI related genes using 4 methods:

3.4.1 Method 1: WGCNA Analysis and Hub IRI Related Genes

We performed WGCNA analysis on GSE98622, GSE52982 & GSE65656. We set the β value (power value) as 1-30, and calculated the corresponding correlation coefficient and gene adjacency function mean (Figure 7A-D). In GSE98622, when β was 26, the established network was closest to the scale-free network, while in GSE52982&GSE65656, when β was 28, it was the closest to the scale-free network.

After selecting the β value as the network construction parameter, we established a weighted co-expression network model, and then used the Dynamically cut tree algorithm to mine modules. We set at least 100 genes in each module in GSE98622, and the maximum connection height as 0.95 (i.e., the parameters minModuleSize = 100 and cutHeight = 0.95 in the cutreeDynamic method). In GSE52982&GSE65656, there were at least 30 genes in each module, and the maximum junction height was 0.95. After obtaining the modules, we merged the modules with correlation coefficients greater than 0.8 (Figure 7E-F).

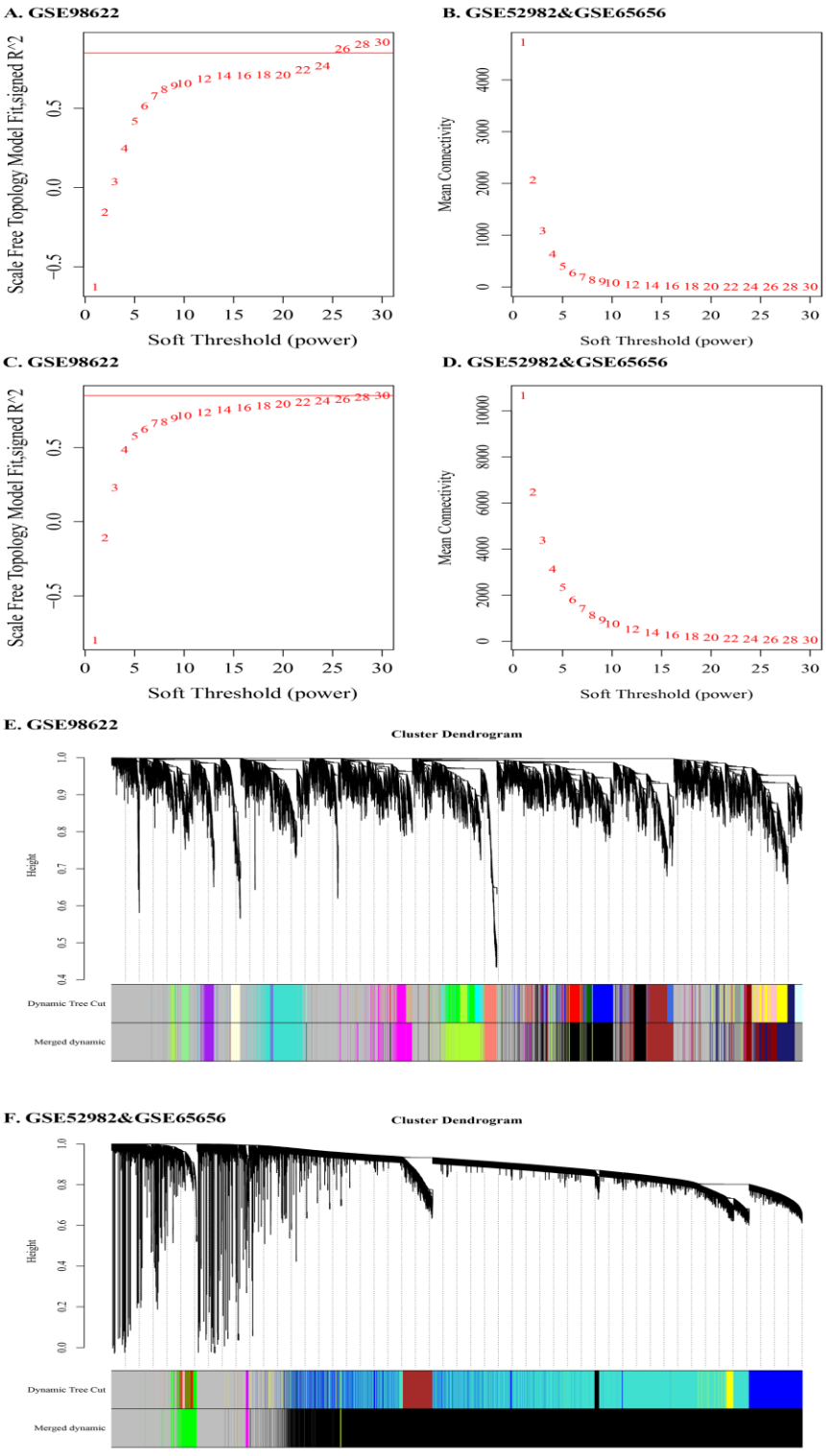

Figure 7. WGCNA Analysis Results. (A) and (C) are the correlation coefficients corresponding to different β values. (B) and (D) are the average connectivity of networks constructed with different β values. (E-F) are the results of module mining. Each black line in the upper half represents a gene, the lower half is the module where the gene is located. Dynamic Tree Cut is the module obtained initially, and Merged dynamic is the module after combining modules with correlation coefficients greater than 0.8.

We extracted the modules where the DEGs were located and screened for significant modules based on the differentially expressed P.adjust value (Figure 8A-C). For the case vs control group of GSE98622, we obtained turquoise as a significant module (Figure 8A). For the case vs sham group of GSE98622, we obtained black as a salient module (Figure 8B). The salient modules obtained by GSE52982 & GSE65656 were green and black, respectively (Figure 8C). We extracted the IRI related genes under the salient modules and obtained a total of 26 IRI related genes in GSE98622 (Figure 8D) and 13 IRI related genes in GSE52982&GSE65656 (Figure 8E).

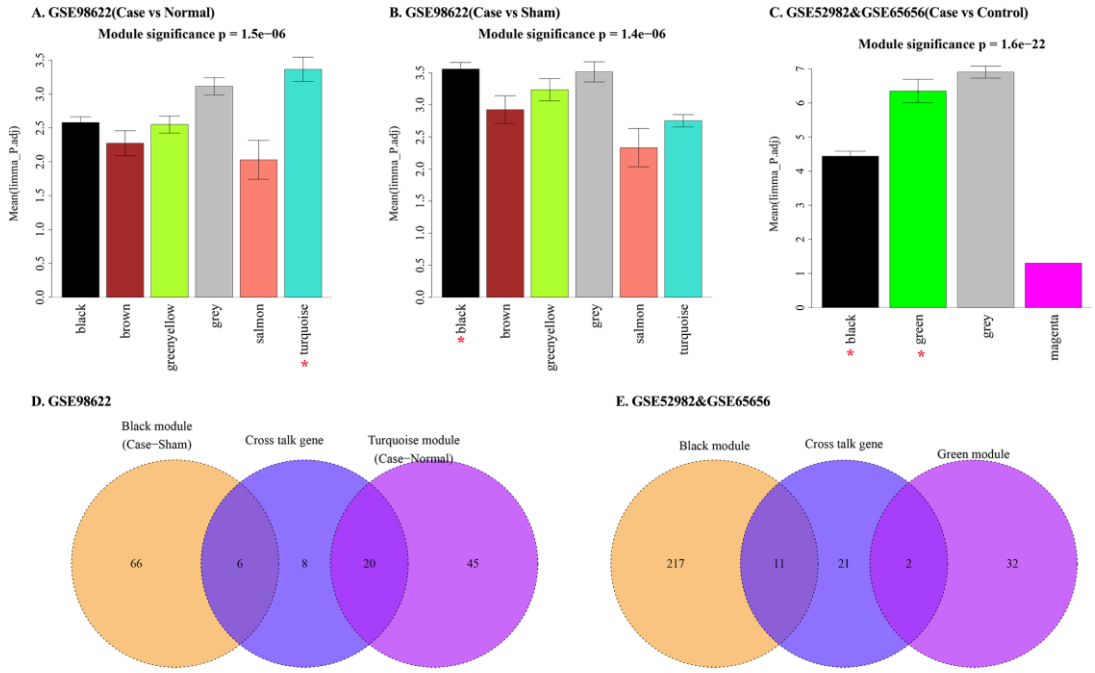

Figure 8. Screening IRI Related Genes by Module Significance Analysis. (A-C) Significance analysis of GSE98622 and GSE52982&GSE65656 modules based on differentially expressed P.adjust values; (D-E) Intersection of IRI related genes and significant module genes in GSE98622 and GSE52982&GSE65656.

In the correlation analysis of IRI related genes and all modules, the results obtained for the GSE98622 significant module black IRI related genes and black, greenyellow, turquoise correlation was higher; IRI related genes in the significant module turquoise and black, greenyellow, turquoise, salmon had a higher correlation (Figure 9A). In GSE52982 & GSE65656, the IRI related genes in the salient module black were highly correlated with black, greenyellow, and green, and the IRI related genes in the salient module green had higher correlations with black, greenyellow, and green (Figure 9B). We obtained IRI related genes that existed in significant modules of GSE98622, GSE52982 & GSE65656, and finally obtained 11 WGCNA-related Hub genes (Acsm3, Akr1c14, Aldh1a2, Bcat1, C3, Cyp2d9, Hpd, Kdelr3, Neurog2, Pigr, Slc22a7) (Figure 9C).

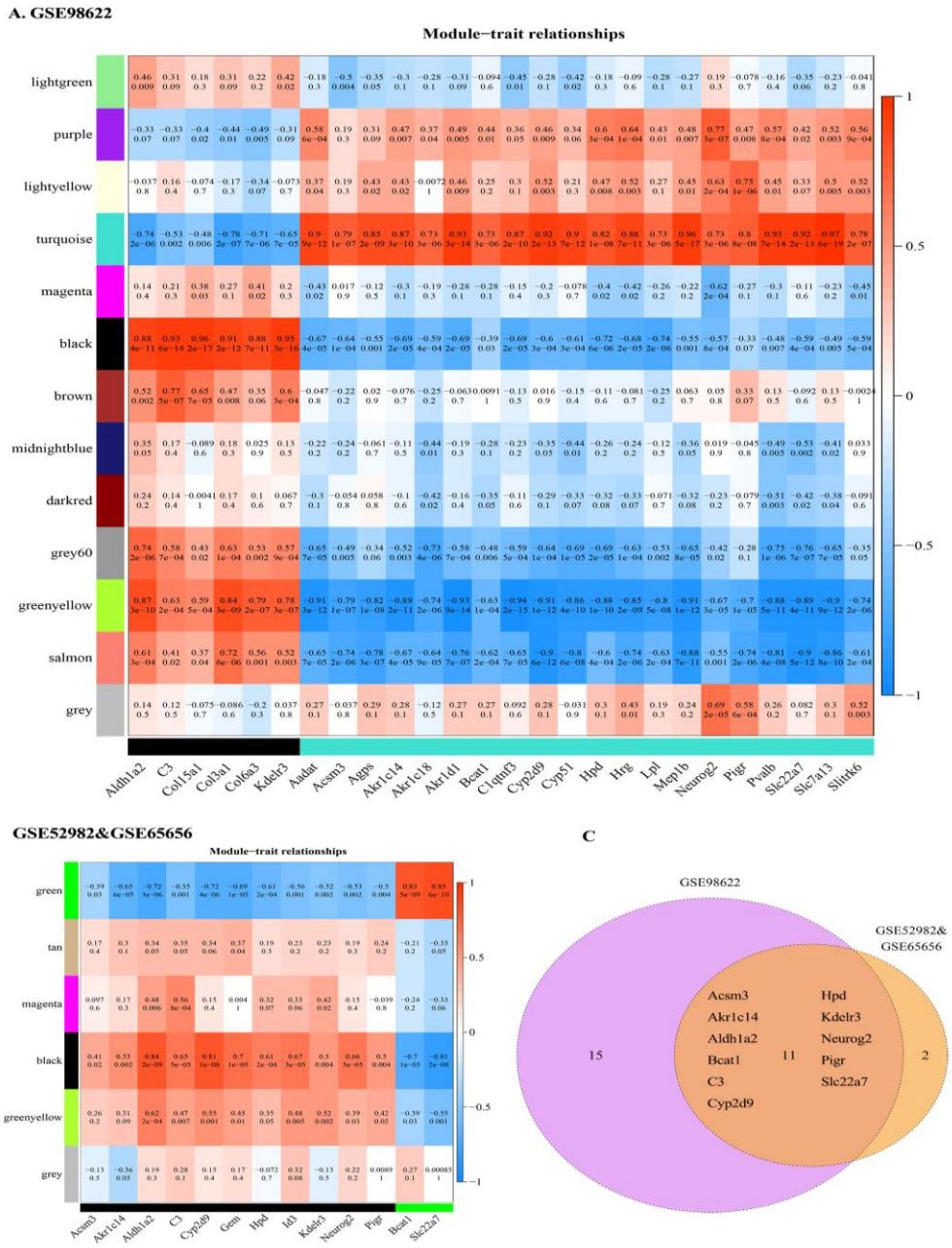

Figure 9. IRI Related Gene and Module Correlation Analysis. (A-B) Correlation heatmaps showing the relationship between IRI related genes and significant modules in GSE98622 and GSE52982&GSE65656. The abscissa represents the IRI related genes under the significant module, the color bar above shows the module assignment, and the ordinate represents all modules obtained by WGCNA. (C) Venn diagram showing IRI-related genes common in significant modules of GSE98622 and GSE52982&GSE65656, resulting in 11 WGCNA-related hub genes.

3.4.2 Method 2: Immune Infiltration Analysis on IRI Samples and Correlated Hub Genes

We obtained the corresponding human gene DEG expression matrix through the homology alignment of GSE98622, GSE52982 & GSE65656 genes. GSE98622, GSE52982 & GSE65656 were subjected to

immune infiltration analysis using ESTIMATE to obtain the sample fractions of stromal cells and immune cells. We used the Wilcoxon test to test the differences in immune cells in different samples in GSE98622, GSE52982 & GSE65656. Stromal cells were significantly different in different samples of GSE98622 and GSE52982 & GSE65656 (Figure 10A, Figure 10B). There were no differences in immune cells among different groups of GSE98622 samples (Figure 10C), but significant differences among different samples of GSE52982 & GSE65656 (Figure 10D).

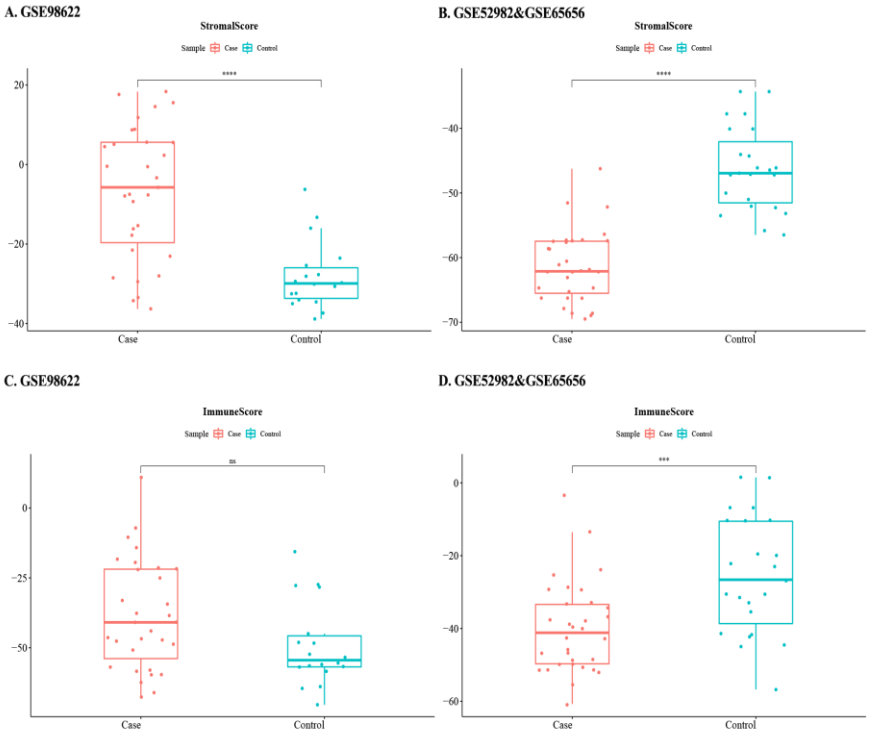

Figure 10. Differential Enrichment of Stromal Cells and Immune Cells. (A-B) Differential enrichment of stromal cells in GSE98622 and GSE52982&GSE65656 samples. (C-D) Differential enrichment of immune cells in GSE98622 and GSE52982&GSE65656 samples. Statistical significance is indicated by asterisks: ns: $p > 0.05$, *: $p \leq 0.05$, **: $p \leq 0.01$, ***: $p \leq 0.001$, ****: $p \leq 0.0001$.

We performed ROC analysis on stromal cells and immune cells in GSE98622 and GSE52982 & GSE65656. The ROC for stromal cells in GSE98622 and GSE52982 & GSE65656 was better, while the ROC for immune cells in GSE98622 and GSE52982 & GSE65656 was poor (Figure 11A, Figure 11B). From this, it can be obtained that stromal cells and immune cells are differently implicated in IRI, and suggest that IRI may have a relatively large impact on stromal cells but a small impact on immune cells. Then we used the Pearson correlation coefficient to analyze the relationship between the two cell types and the IRI related genes in the Case-samples (Figure 11C). 16 Hub IRI related genes related to immune infiltration (Aadat, Aldh1a2, Basp1, Bcat1, C3, Col3a1, Col15a1, Cyp2d9, Fos, Gem, Hpd, Id3, Mep1b, Pigr, Slc22a7, Slc7a13) were obtained (Figure 11C).

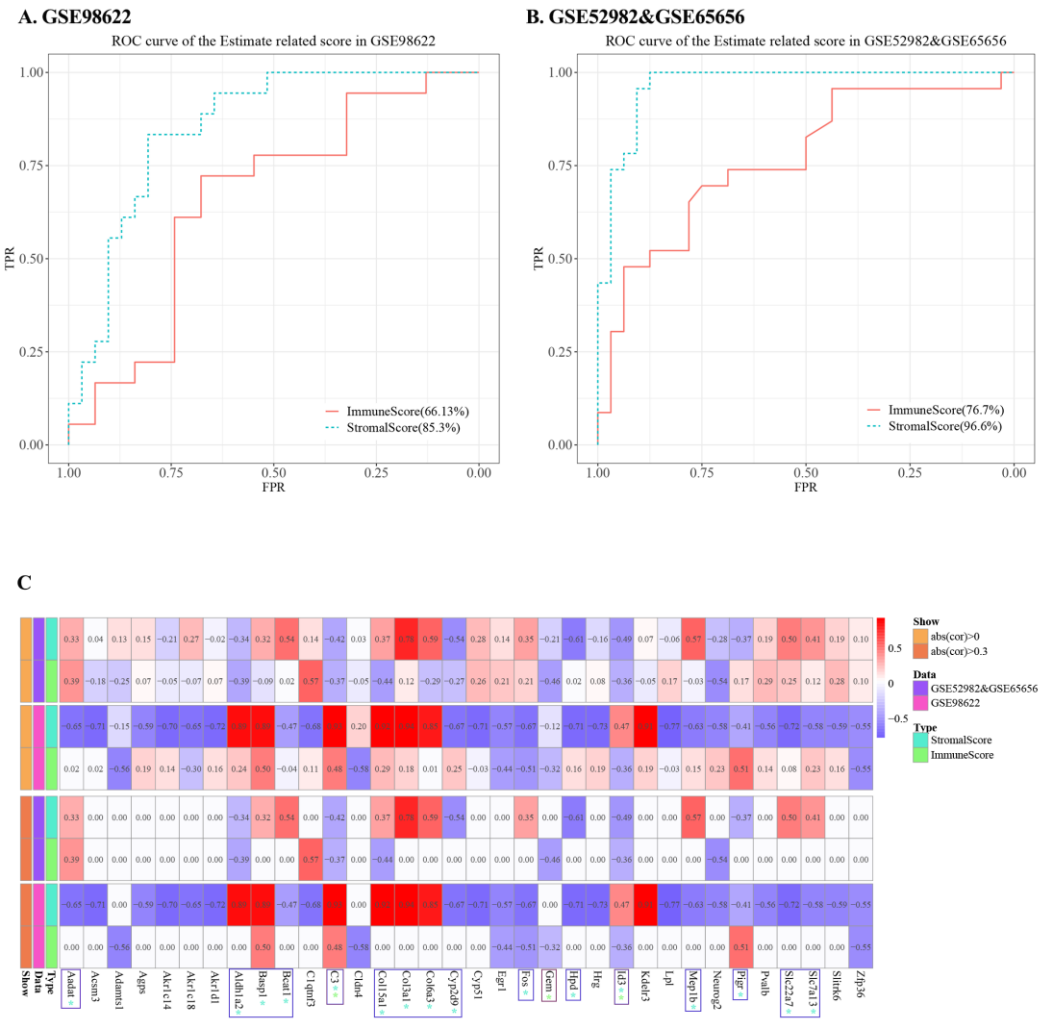

Figure 11. ROC and Correlation Analysis of ESTIMATE. (A-B) ROC analysis of stromal cells and immune cells in GSE98622 and GSE52982&GSE65656. (C) Correlation heatmap of stromal cells and immune cells with IRI related genes in case samples. The upper part shows all correlation results, and the lower part shows only results with |correlation| > 0.3. Genes highly related to stromal cells or immune cells are marked with *.

3.4.3 Method 3: Screening of Hub IRI Related Genes by ANOVA and LASSO

We performed ANOVA analysis on the GSE98622 and GSE52982 & GSE65656 datasets respectively, and obtained 34 IRI-related genes that were differentially expressed in GSE98622 and GSE52982 & GSE65656 (Figure 12A). Then we used LASSO Logistic Regression to further screen 34 IRI related genes. For GSE98622 we obtained 12 feature genes (Figure 12B). For GSE52982 & GSE65656, we obtained 14 feature genes (Figure 12C). We intersected the feature genes obtained from the two datasets to obtain 6 Hub IRI related genes (Aldh1a2, Basp1, Bcat1, Fos, Id3, Slitrk6) (Figure 12D).

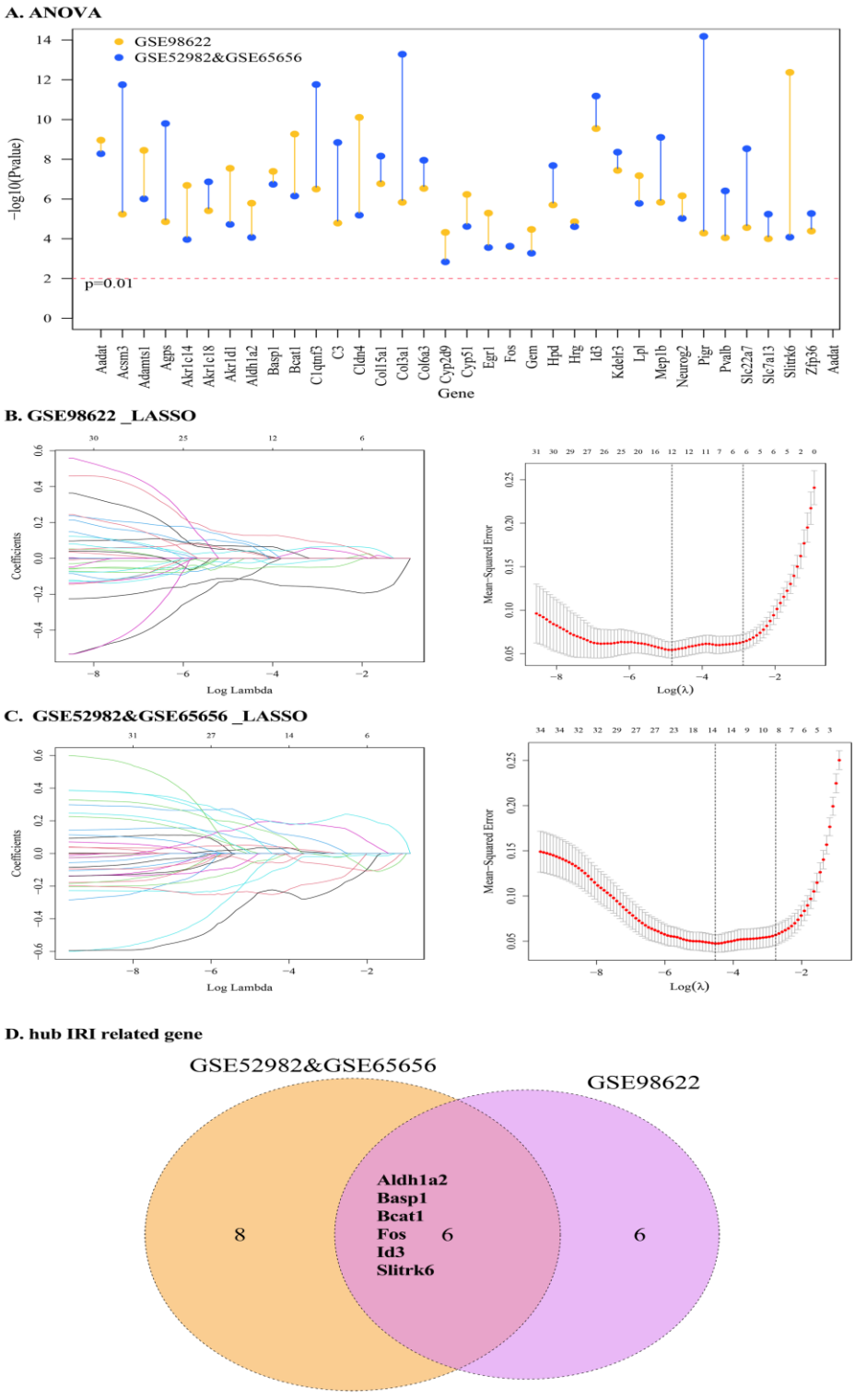

Figure 12. LASSO Analysis to Screen Hub IRI Related Genes. (A) Results of ANOVA analysis on GSE98622 and GSE52982&GSE65656 datasets. (B-C) LASSO analysis results. The left panels show LASSO coefficient paths, and the right panels show cross-validation results with lambda.min and lambda.1se values indicated. (D) Venn diagram showing the intersection of hub IRI related genes obtained after LASSO analysis from both datasets.

3.4.4 Method 4: Screening of Hub IRI Related Genes by Consensus Cluster Plus

We used Consensus Cluster Plus (Wilkerson et al., 2010) to perform cluster analysis on GSE98622 and GSE52982 & GSE65656. The results showed that when k=4 in GSE98622, the clustering effect was the best (Figure 13A, Figure 13C). When k=4 in GSE52982&GSE65656, the clustering effect was the best (Figure 13B, Figure 13D). When k=4, the consistent clustering results for GSE98622 and GSE52982 & GSE65656 are shown in Figure 13E and Figure 13F.

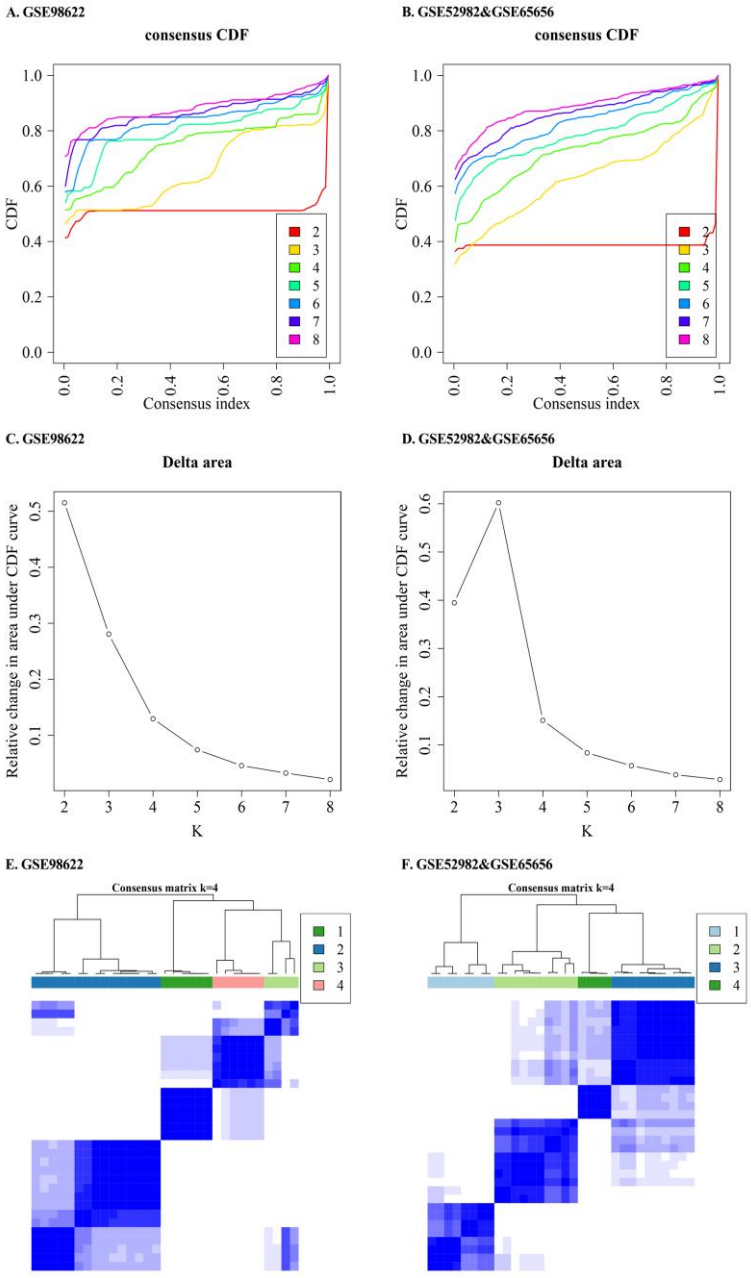

Figure 13. Consensus Cluster Plus Analysis Results. (A-B) Concordant cumulative distribution function (CDF) plots showing optimal clustering when k=4. (C-D) Relative change in area under the CDF curve for different k values. (E-F) Consistent clustering heatmaps for GSE98622 and GSE52982&GSE65656 when k=4.

We performed multi-group differential expression analysis of IRI related genes according to Cluster. We selected IRI related genes with Pvalue <0.05 in GSE98622 and GSE52982 & GSE65656 as differentially expressed IRI related genes, and then took the intersection of the differential IRI related genes. Finally, we obtained 4 Hub genes (Col3a1, Pigr, Cyp2d9, Hpd) related to Consensus Cluster Plus (Fig 14A). We used boxplots to show the expression of these genes in different clusters of GSE98622 and GSE52982 & GSE65656 (Fig 14B-C). At the same time, kruskal.test was used to analyze the differences of hub IRI related genes in different clusters. The results showed that four hub IRI related genes were significantly different in the different clusters.

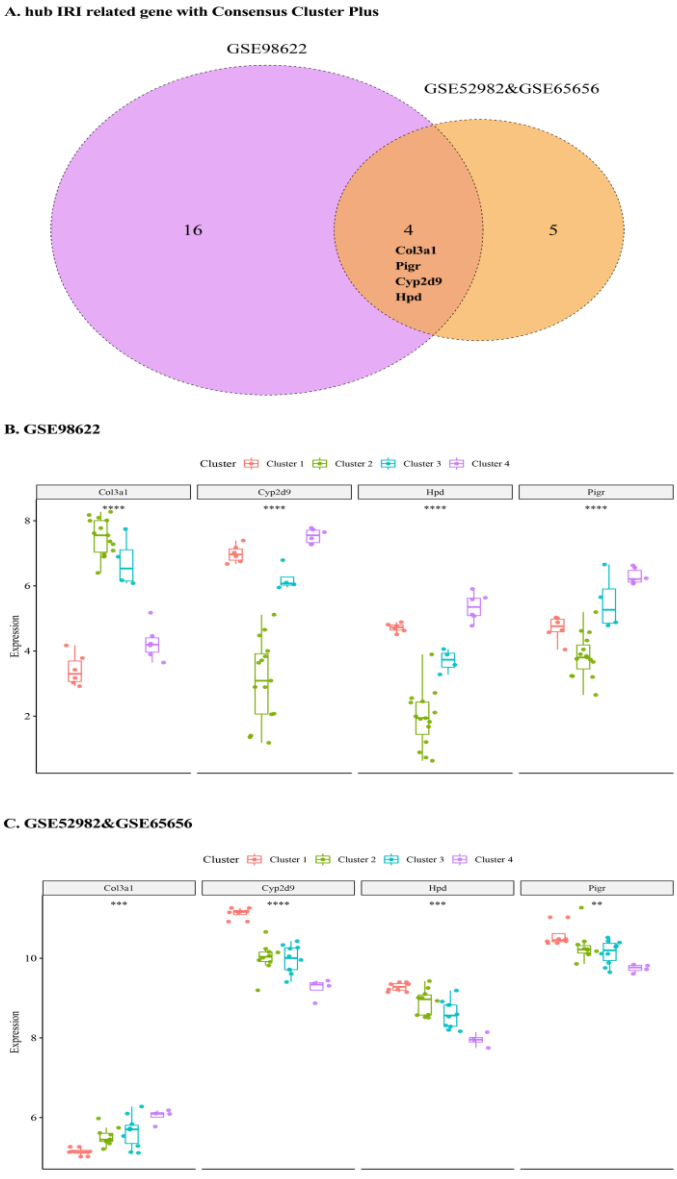

Figure 14. Hub Genes Related to Consensus Cluster Plus. (A) Venn diagram showing hub genes associated with Consensus Cluster Plus analysis. (B-C) Boxplots showing the expression of hub IRI related genes in different clusters of GSE98622 and GSE52982&GSE65656. Statistical significance was determined using Kruskal-Wallis test.

Through the above four methods, we obtained hub IRI related genes under each method. In order to obtain a more accurate hub IRI related gene set, we selected hub IRI related genes that appeared in any of the three methods as the significant hub IRI related genes. Finally, 5 hub IRI related genes (Hpd, Cyp2d9, Aldh1a2, Pigr, Bcat1) were obtained. We extracted the expression values of the 5 hub IRI related genes in GSE98622 and GSE52982 & GSE65656, and performed the Wilcoxon Test. The hub IRI related genes were verified to be different between diseased and normal samples (Figure 15B, Figure 15C). Then, ROC analysis was performed and it was found that the AUC values of the five genes were relatively high (Figure 15D, Figure 15E). It can be concluded that the five hub genes are likely to have significant discriminant ability for both conventional IRI and diet-controlled IRI experiments.

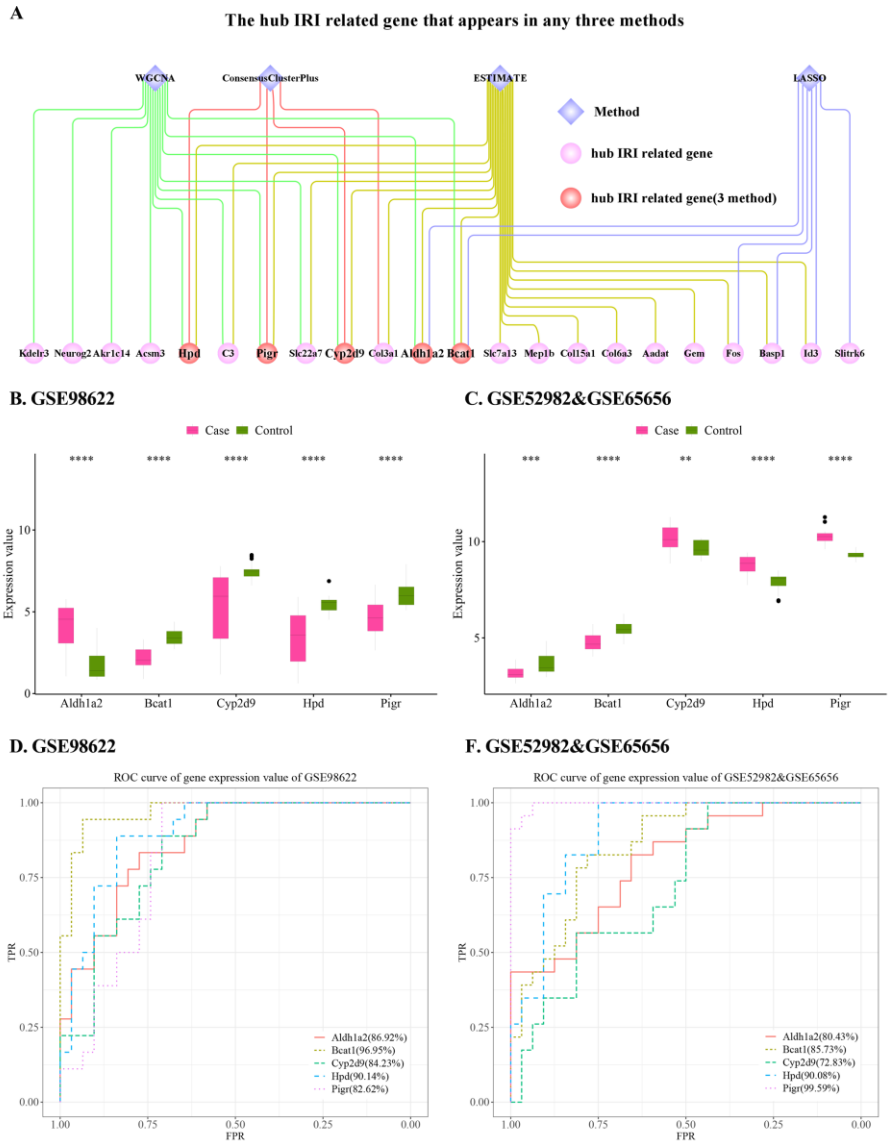

Figure 15. Analysis of Significant Hub IRI Related Genes. (A) Workflow diagram showing the screening of hub IRI related genes by four methods, resulting in five consensus genes. (B-C) Expression values of five significant IRI related genes in case and control samples. (D-E) ROC analysis results showing high AUC values for the five significant IRI related genes.

3.5 SVM Analysis of Significant Hub IRI Related Genes

We obtained the expression values of 5 significant hub IRI related genes (Hpd, Cyp2d9, Aldh1a2, Pigr, Bcat1) in GSE98622 and GSE52982&GSE65656. The expression values for GSE98622 and GSE52982 & GSE65656 were then combined. In performing SVM analysis, we used 70% of the combined samples for model training and 30% for model validation. After training the model, we input the training set and test set into the models to obtain sample scores, and performed ROC analysis on the sample scores to assess the effect (Figure 16A).

At the same time, we performed SVM analysis on these five significant hub IRI related genes for the three datasets GSE39548, GSE182793 and GSE142077. Finally, we combined six datasets; GSE98622, GSE52982 & GSE65656, GSE39548, GSE182793 and GSE142077, and constructed an SVM model to analyze the prediction effects of these five consensus hub IRI related genes. Since the 5 consensus hub related genes were not present in all datasets, we used 3 shared hub genes (Hpd, Aldh1a2, Pigr) that appeared in all datasets for the analysis. The results obtained in the combined dataset of GSE98622 and GSE52982 & GSE65656, with the SVM training set and validation set based on 5 significant hub related genes showed very high values (AUC>90%, Figure 16A). In the combined dataset of GSE39548, GSE182793 and GSE142077, the SVM training set and test set established based on 3 significant hub related genes performed well (AUC>88%, Figure 16B). When we combining the six datasets GSE98622, GSE52982 & GSE65656, GSE39548, GSE182793 and GSE142077, the SVM prediction model showed AUCs obtained for both the training set and the test set as greater than 85% (Figure 16C).

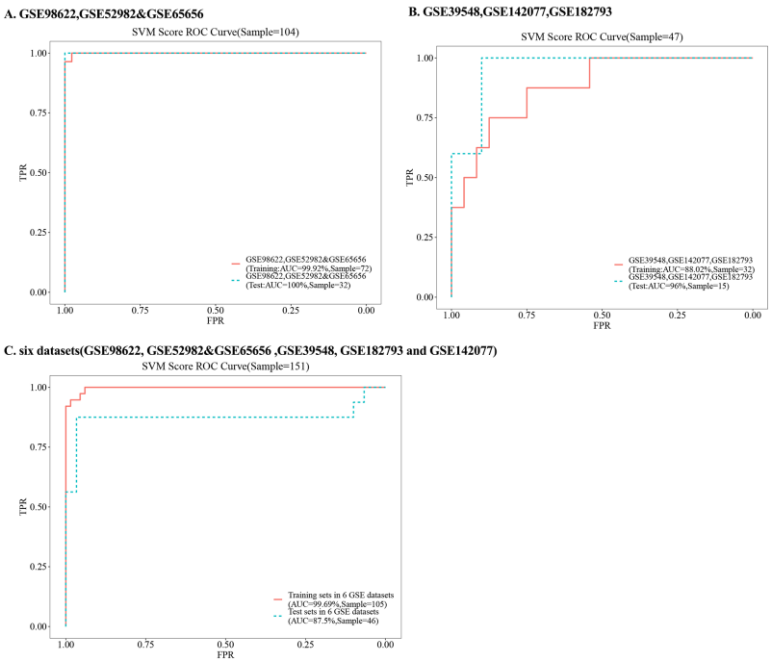

Figure 16. SVM Model Prediction Effect of 5 Significant Hub IRI Related Genes. (A) Combined dataset of GSE98622 and GSE52982&GSE65656; (B) Combined dataset of GSE39548, GSE182793 and GSE142077; (C) Combined dataset of all six datasets. All models show AUC values greater than 85%, indicating robust predictive performance.

All 3 SVMs had good prediction ability, which indicated that the 5 consensus hub genes are likely to be key players in IRI. In addition, we analyzed the correlation of 5 significant hub IRI related genes (Hpd, Cyp2d9, Aldh1a2, Pigr, Bcat1) in GSE98622 and GSE52982 & GSE65656.The results depicted several significant gene-gene correlations and showed that Cyp2d9 was highly correlated with Hpd and Pigr in GSE98622 and GSE52982 & GSE65656 (Figure 17, Figure 18).

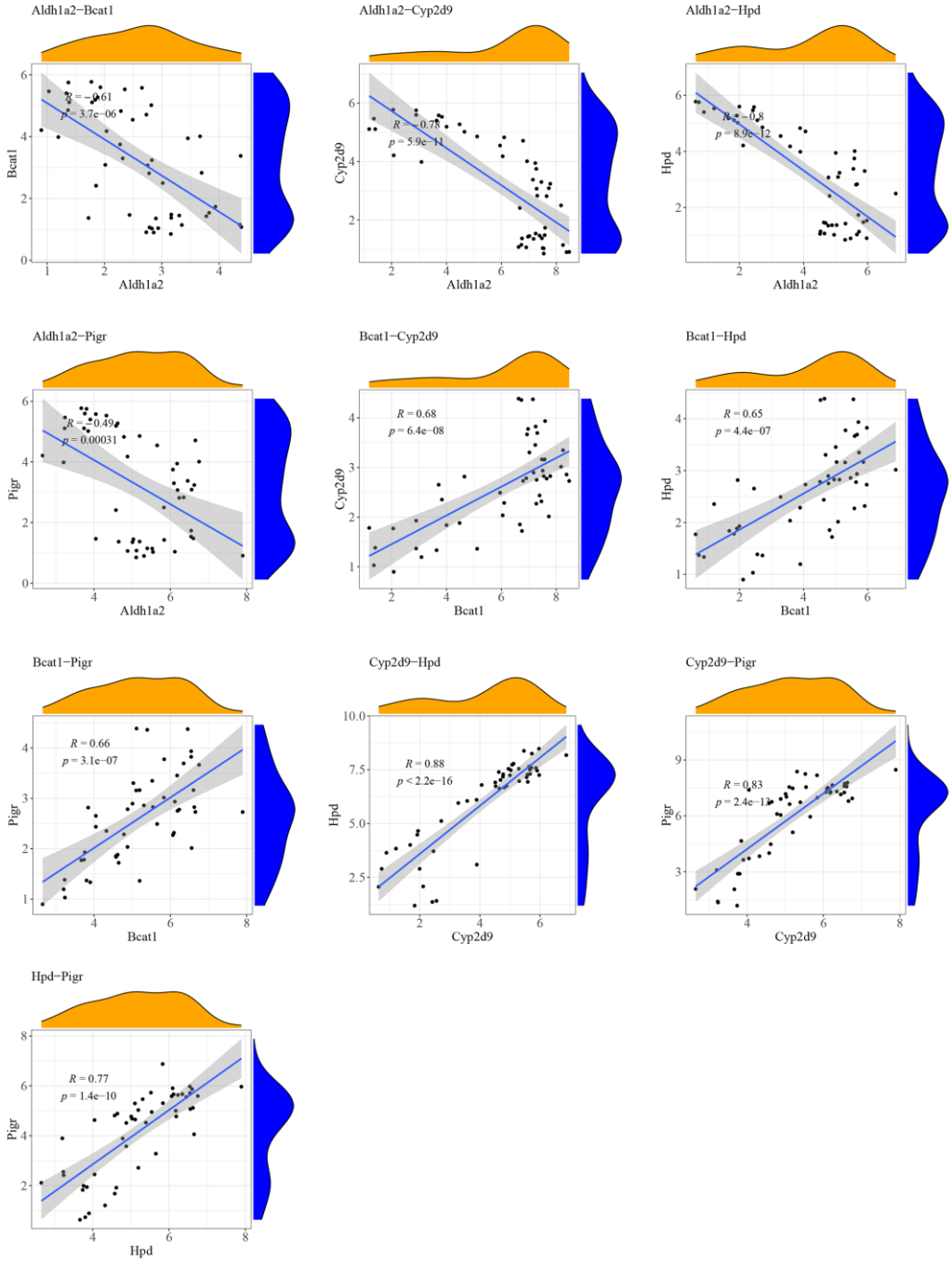

Figure 17. Correlation of 5 Significant Hub IRI Related Genes in GSE98622. Scatter plots with correlation coefficients showing pairwise relationships between the five hub genes. Cyp2d9 shows high correlation with Hpd (R=0.98) and Pigr (R=0.93).

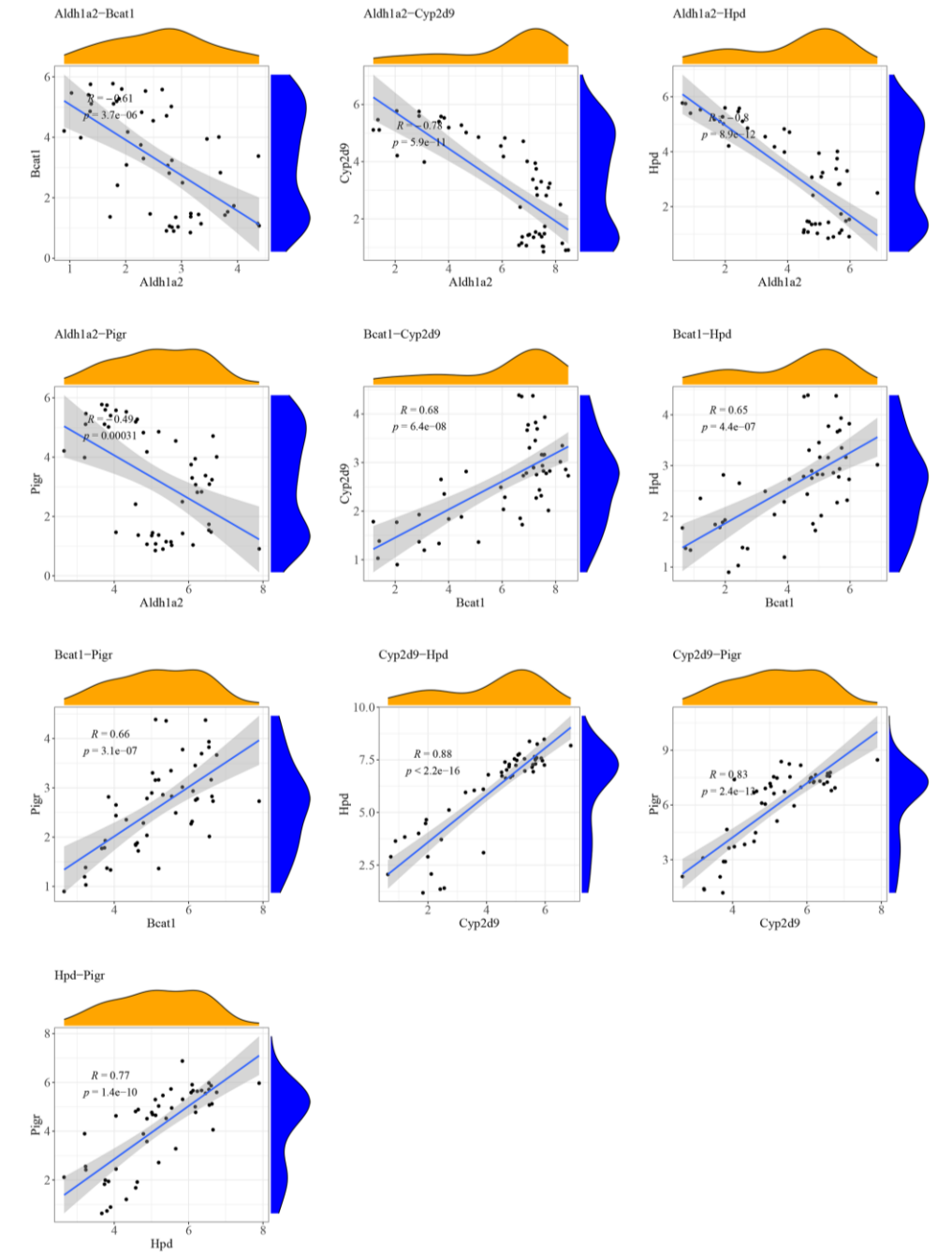

Figure 18. Correlation of 5 Significant Hub IRI Related Genes in GSE52982 & GSE65656. Scatter plots showing similar correlation patterns as in GSE98622, with Cyp2d9 highly correlated with Hpd (R=0.88) and Pigr (R=0.91).

3.6 Hub Gene-DEmiRNA-lncRNA Network Analysis

We downloaded the IRI-related miRNA dataset GSE29495 from the GEO database, which contains 569 miRNAs. We performed differential expression analysis of GSE29495 using the "limma" package for R. We screened miRNAs with P.adjust<0.01 and |log2FC|>2.5 as DEmiRNAs, and obtained a total of 473 DEmiRNAs. We then predicted DEmiRNAs targeting significant hub IRI related genes from miRWalk

(http://mirwalk.umm.uni-heidelberg.de/) and obtained DEmiRNA-regulated lncRNA relationship pairs from ENCORI (https://starbase.sysu.edu.cn/). For DEmiRNA-significant hub IRI related gene relationship pairs, and DEmiRNA-lncRNA relationship pair integration, we finally obtained the hub gene-DEmiRNA-lncRNA relationship pairs. We used Cytoscape (version 3.8) software to construct a hub gene-DEmiRNA-lncRNA network (Figure 19A). The hub gene-DEmiRNA-lncRNA network consists of 118 nodes and 247 edges. The 118 nodes contained 4 Hub genes, 37 DEmiRNAs and 77 lncRNAs. From the regulatory relationships, it can be obtained that Bcat1 is regulated by multiple DEmiRNAs, potentially playing an important role in altered biological function. We computed the Pearson correlation coefficient to analyze the relationships between the 37 miRNAs based on GSE29495 expression values. The results obtained showed highly positive correlations between miRNAs in the IRI experiments.

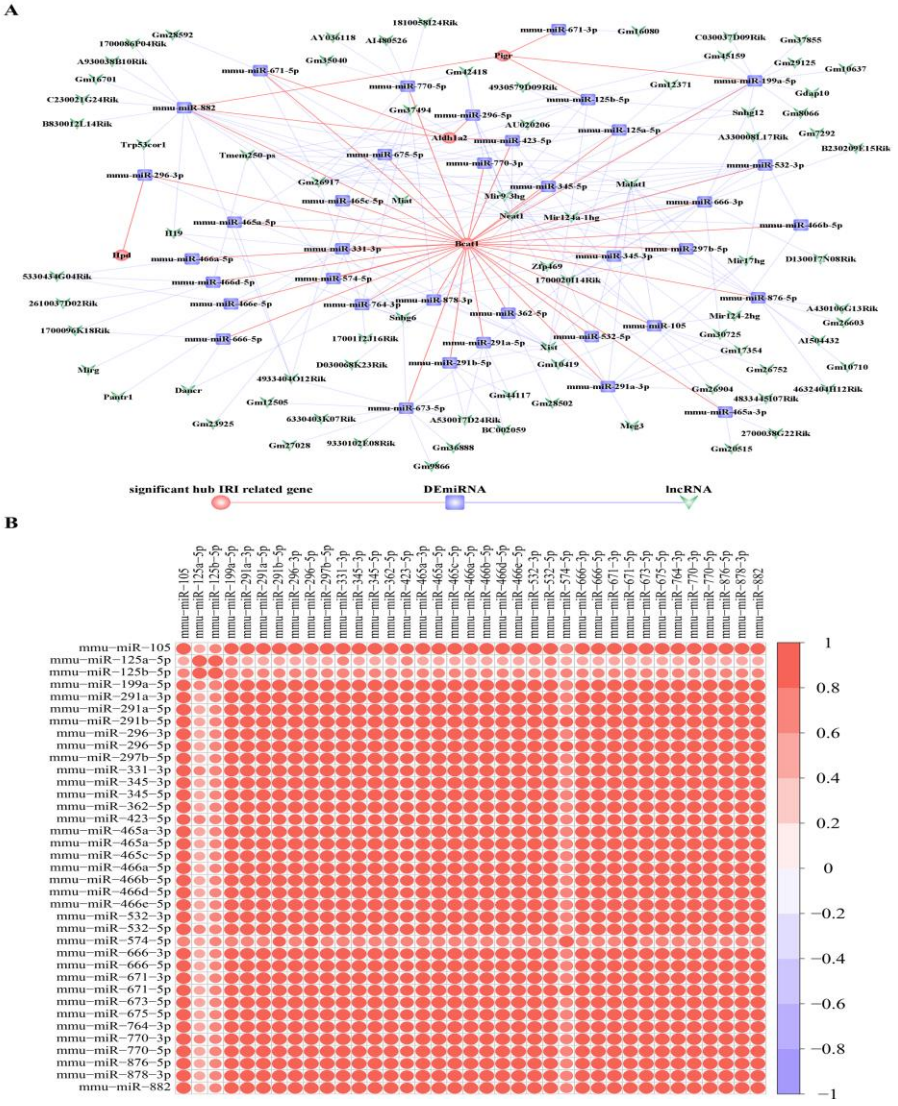

Figure 19. DEmiRNA-related Regulatory Networks and Correlations. (A) Hub gene-DEmiRNA-lncRNA network constructed using Cytoscape, consisting of 118 nodes (4 hub genes, 37 DEmiRNAs, 77 lncRNAs) and 247 edges. Bcat1 shows regulation by multiple DEmiRNAs. (B) Correlation heatmap showing positive correlations between the 37 miRNAs in GSE29495.

4. Discussion

In the present study, using a suite of bioinformatics analyses we integrated multiple gene expression datasets and applied four different screening tools to identify the most relevant deregulated genes in renal IRI. Here, we integrated multiple datasets from IRI under conventional and dietary restriction conditions and identified 5 gene features with high predictive values. The analytical pipeline consisted of identification of IRI-related genes via differential gene expression analysis and functional enrichment analysis, followed by feature selection for hub IRI related genes using 4 different approaches based on discrete theoretical bases; WGCNA analysis, immune infiltration analysis, LASSO regression and Consensus Cluster Plus. This approach allowed the application of feature selection tools using different perspectives to identify key deregulated genes. WGCNA harvests pair-wise correlations to identify highly correlated gene modules, their association with metadata variables, and hub gene identification (Langfelder et al., 2008). Immune cell infiltration analysis was done using ESTIMATE algorithm derived immune scores (Ma et al., 2021) and correlating IRI related genes in case samples comprised a gene signature. This approach was directed at identifying key genes linked to immune and stromal cell deregulations in the IRI microenvironment. LASSO is a regularization based regression approach that has been widely used for biomarker discovery as it permits model and feature selection both (Tibshirani, 1996; Owzar et al., 2011) Consensus cluster plus is a tool that permits unsupervised class discovery (Wilkerson & Hayes, 2010). Integrating these diverse biomarker discovery approaches we identified a gene-signature for IRI.

The 5 IRI related genes that emerged as consensus genes identified by the 4 methods included Hpd, Cyp2d9, Aldh1a2, Pigr and Bcat1. The Hpd gene encodes for an enzyme 4-hydroxyphenylpyruvate dioxygenase, which is involved in tyrosine catabolism and is expressed in renal epithelial cells, as tyrosine is also degraded in the kidney and Hpd deregulation can produce renal tubular cell apoptosis (Endo & Sun, 2002). The Cyp2d9 codes for cytochrome P450, family 2, subfamily d, polypeptide 9 is located in the mitochondrion and found primarily in the liver, and renal injury in IRI shows marked degradation of cytochrome P450 proteins (Nakao et al., 2008; Renaud et al., 2011). Cyp2d9 genotype has been linked to adverse drug reactions after renal transplant (Miroševic et al., 2013). Aldh1a2 or aldehyde dehydrogenase 1 family, member A2 is involved in the retinoic acid pathway and is implicated in renal development (El Kares et al., 2010). Retinoic acid signaling in the tubular epithelium is protective in acute kidney injury by limiting macrophage-induced damage (Chiba et al., 2016). The polymeric Ig receptor (PIgR) is expressed in proximal tubular cells and glomerular parietal epithelial cells mediating the transport of secretory IgA (Rice et al., 1999). In diseased state, its expression in proximal tubular cells is upregulated in association with urinary secretory IgA levels, whereas it is downregulated in ischemia (Krawczyk et al., 2019). Branched chain amino acid transaminase 1 (Bcat1) activity is highly abundant in the kidney (Ichihara et al., 1966). Branched chain amino acid (BCAA) metabolism is implicated in IRI by promoting lipid peroxidation and deregulating glucose oxidation (Li et al., 2020). The restriction of BCAAs is a mode for dietary inhibition of the m-TOR pathway that results in improved resistance to

oxidative stress ((Fontana et al., 2016; Robertson et al., 2015). Bcat1 is shown to participate in m-TOR regulation via the PI3K/AKT/mTOR pathway (Shu et al., 2021). We found that Bcat1 was regulated by multiple DEmiRNAs. Thus, dietary protein restriction might downregulate Bcat1-mTOR signaling to attenuate renal IRI. In a related finding, KEGG pathway analysis showed protein digestion and absorption and BCAAs valine, leucine and isoleucine biosynthesis as enriched pathways in renal IRI.

Functional enrichment analysis of the IRI related genes showed the highest enrichment of biological processes including cellular hormone metabolic process, progesterone metabolic process, carboxylic and organic acid biosynthesis processes. Progesterone receptors are implicated in ascorbic acid mediated protection from acute renal IRI (Sandhi et al., 2014). Bioactive oxidized phosphatidylcholine including carboxylic acid containing species are produced in renal IRI and correlate with the duration and severity of injury (Solati et al., 2018). The 2-Oxocarboxylic acid metabolism KEGG pathway was also found enriched. The AGE-receptor for advanced glycation endproducts (RAGE) signaling pathway in diabetes was among the top enriched pathways. Diabetes is an important risk factor for renal IRI, and in hyperglycemia AGE-RAGE signaling promotes oxidative damage in renal IRI (Leu et al., 2021). RAGE and its ligand High-mobility group box-1 (HMBG1) are mediated in IRI of several tissues (Zeng et al., 2004) and in renal inflammation but not consistently associated with injury in renal IRI (Dessing et al., 2012).

Despite the comprehensive approach and valuable findings, this study has several limitations that warrant acknowledgment. First, the analysis was entirely based on publicly available transcriptomic datasets, which may introduce heterogeneity due to different experimental protocols, platforms, and batch effects, despite our efforts to normalize and correct for these variations. Second, our findings are primarily derived from mouse models, which may not fully recapitulate the complexity of human renal IRI, particularly given species-specific differences in metabolism and immune response. Third, the validation datasets used were limited, and experimental validation in independent cohorts or clinical samples was not performed. Additionally, our approach focused on mRNA expression levels and did not account for post-transcriptional modifications, protein abundance, or functional activity of the identified hub genes. Finally, the temporal dynamics of gene expression during IRI progression were not fully captured, as most datasets represented single time points rather than longitudinal changes throughout the ischemia-reperfusion process.

The identification of five consensus hub genes (Hpd, Cyp2d9, Aldh1a2, Pigr, Bcat1) presents significant potential for clinical translation in renal transplantation and acute kidney injury management. These genes could serve as prognostic biomarkers for early detection of IRI, enabling clinicians to implement timely interventions and personalized treatment strategies. The robust performance of these genes in SVM models (AUC >85-90%) suggests their utility as a diagnostic panel for risk stratification in kidney transplant recipients. From a therapeutic perspective, the pathways associated with these genes—particularly BCAA metabolism, retinoic acid signaling, and cytochrome P450 function—represent actionable targets for pharmacological intervention. Future research should focus on

validating these findings in clinical cohorts, developing non-invasive detection methods (such as urinary biomarkers), and investigating targeted therapeutic approaches. Additionally, exploring the temporal expression patterns of these genes throughout IRI progression could inform optimal timing for interventions. The integration of these molecular signatures with clinical variables and imaging data could enable the development of predictive models for IRI severity and recovery outcomes, ultimately improving transplant success rates and patient care.

Together, the present study identified the most relevant genes and functional processes implicated in the pathogenesis of renal IRI using a rigorous, consensus-based feature selection approach applied to leverage multiple gene expression datasets. These genes can be considered valuable biomarker and therapeutic target candidates and should be validated in experimental and clinical research models.

5. Conclusion

Integrative bioinformatics analysis of multiple gene expression datasets pertaining to renal IRI under conventional and dietary restriction conditions was performed with a consensus-based approach for discriminant feature selection. A set of 5 genes: Hpd, Cyp2d9, Aldh1a2, Pigr, Bcat1 were identified as the top candidate biomarker and therapeutic targets in renal IRI.

References

Baines, C. P. (2009). The mitochondrial permeability transition pore and ischemia-reperfusion injury. *Basic research in cardiology*, *104*(2), 181-8. https://doi.org/10.1007/s00395-009-0004-8

Chiba, T., Skrypnyk, N. I., Skvarca, L. B., Penchev, R., Zhang, K. X., Rochon, E. R., Fall, J. L., Paueksakon, P., Yang, H., Alford, C. E., & Roman, B. L. (2016). Retinoic acid signaling coordinates macrophage-dependent injury and repair after AKI. *Journal of the American Society of Nephrology*, *27*(2), 495-508. https://doi.org/10.1681/ASN.2014111108

Dessing, M. C., Pulskens, W. P., Teske, G. J., Butter, L. M., Van Der Poll, T., Yang, H., Tracey, K. J., Nawroth, P. P., Bierhaus, A., Florquin, S., & Leemans, J. C. (2012). RAGE does not contribute to renal injury and damage upon ischemia/reperfusion-induced injury. *Journal of innate immunity*, *4*(1), 80-5. https://doi.org/10.1159/000334251

El Kares, R., Manolescu, D. C., Lakhal-Chaieb, L., Montpetit, A., Zhang, Z., Bhat, P. V., & Goodyer, P. (2010). A human ALDH1A2 gene variant is associated with increased newborn kidney size and serum retinoic acid. *Kidney international*, *78*(1), 96-102. https://doi.org/10.1038/ki.2010.101

Endo, F., & Sun, M. S. (2002). Tyrosinaemia type I and apoptosis of hepatocytes and renal tubular cells. *Journal of inherited metabolic disease*, *25*(3), 227-34. https://doi.org/10.1023/A:1015646400182

Feng, W., Tang, R., Ye, X., Xue, C., & Liao, Y. (2016). Identification of genes and pathways associated with kidney ischemia-reperfusion injury by bioinformatics analyses. *Kidney and Blood Pressure Research*, *41*(1), 48-54. https://doi.org/10.1159/000368546

Fontana, L., Cummings, N. E., Apelo, S. I., Neuman, J. C., Kasza, I., Schmidt, B. A., Cava, E., Spelta, F.,

Tosti, V., Syed, F. A., & Baar, E. L. (2016). Decreased consumption of branched-chain amino acids improves metabolic health. *Cell reports*, *16*(2), 520-30. https://doi.org/10.1016/j.celrep.2016.05.092

Franzin, R., Stasi, A., Fiorentino, M., Simone, S., Oberbauer, R., Castellano, G., & Gesualdo, L. (2021). Renal delivery of pharmacologic agents during machine perfusion to prevent Ischaemia-reperfusion injury: from murine model to clinical trials. *Frontiers in Immunology*, *12*, 2687. https://doi.org/10.3389/fimmu.2021.673562

Guo, A., Wang, W., Shi, H., Wang, J., & Liu, T. (2019). Identification of hub genes and pathways in a rat model of renal ischemia-reperfusion injury using bioinformatics analysis of the gene expression omnibus (GEO) dataset and integration of gene expression profiles. *Medical Science Monitor: International Medical Journal of Experimental and Clinical Research*, *25*, 8403. https://doi.org/10.12659/MSM.920364

Ichihara, A., & Koyama, E. (1966). Transaminase of branched chain amino acids I. Branched chain amino acids-α-ketoglutarate transaminase. *The Journal of Biochemistry*, *59*(2), 160-9. https://doi.org/10.1093/oxfordjournals.jbchem.a128277

Jongbloed, F., De Bruin, R. W., Pennings, J. L., Payán-Gómez, C., Van Den Engel, S., Van Oostrom, C. T., De Bruin, A., Hoeijmakers, J. H., Van Steeg, H., IJzermans, J. N., & Dollé, M. E. (2014). Preoperative fasting protects against renal ischemia-reperfusion injury in aged and overweight mice. *PLoS One*, *9*(6), e100853. https://doi.org/10.1371/journal.pone.0100853

Jongbloed, F., Saat, T. C., Verweij, M., Payán-Gómez, C., Hoeijmakers, J. H., van den Engel, S., van Oostrom, C. T., Ambagtsheer, G., Imholz, S., Pennings, J. L., & van Steeg, H. (2017). A signature of renal stress resistance induced by short-term dietary restriction, fasting, and protein restriction. *Scientific reports*, *7*(1), 1-2. https://doi.org/10.1038/srep40901

Kalogeris, T., Baines, C. P., Krenz, M., & Korthuis, R. J. (2012). Cell biology of ischemia/reperfusion injury. *International review of cell and molecular biology*, *298*, 229-317. https://doi.org/10.1016/B978-0-12-394309-5.00006-7

Krawczyk, K. M., Nilsson, H., Nyström, J., Lindgren, D., Leandersson, K., Swärd, K., & Johansson, M. E. (2019). Localization and regulation of polymeric Ig receptor in healthy and diseased human kidney. *The American Journal of Pathology*, *189*(10), 1933-44. https://doi.org/10.1016/j.ajpath.2019.06.015

Langfelder, P., & Horvath, S. (2008). WGCNA: an R package for weighted correlation network analysis. *BMC bioinformatics*, *9*(1), 1-3. https://doi.org/10.1186/1471-2105-9-559

Leu, J. G., Su, W. H., Chen, Y. C., & Liang, Y. J. (2021). Hydralazine attenuates renal inflammation in diabetic rats with ischemia/reperfusion acute kidney injury. *European Journal of Pharmacology*, *910*, 174468. https://doi.org/10.1016/j.ejphar.2021.174468

Li, Y., Xiong, Z., Yan, W., Gao, E., Cheng, H., Wu, G., Liu, Y., Zhang, L., Li, C., Wang, S., & Fan, M. (2020). Branched chain amino acids exacerbate myocardial ischemia/reperfusion vulnerability via

enhancing GCN2/ATF6/PPAR-α pathway-dependent fatty acid oxidation. *Theranostics*, *10*(12), 5623. https://doi.org/10.7150/thno.44836

Ma, Q., Chen, Y., Xiao, F., Hao, Y., Song, Z., Zhang, J., Okuda, K., Um, S. W., Silva, M., Shimada, Y., & Si, C. (2021). A signature of estimate-stromal-immune score-based genes associated with the prognosis of lung adenocarcinoma. *Translational Lung Cancer Research*, *10*(3), 1484. https://doi.org/10.21037/tlcr-21-223

Miroševic Skvrce, N., Božina, N., Zibar, L., Barišic, I., Pejnovic, L., & Macolic Šarinic, V. (2013). CYP2C9 and ABCG2 polymorphisms as risk factors for developing adverse drug reactions in renal transplant patients taking fluvastatin: a case–control study. *Pharmacogenomics*, *14*(12), 1419-31. https://doi.org/10.2217/pgs.13.135

Nakao, A., Faleo, G., Shimizu, H., Nakahira, K., Kohmoto, J., Sugimoto, R., Choi, A. M., McCurry, K. R., Takahashi, T., & Murase, N. (2008). Ex vivo carbon monoxide prevents cytochrome P450 degradation and ischemia/reperfusion injury of kidney grafts. *Kidney international*, *74*(8), 1009-16. https://doi.org/10.1038/ki.2008.342

Owzar, K., Barry, W. T., & Jung, S. H. (2011). Statistical considerations for analysis of microarray experiments. *Clinical and translational science*, *4*(6), 466-77. https://doi.org/10.1111/j.1752-8062.2011.00309.x

Renaud, H. J., Cui, J. Y., Khan, M., & Klaassen, C. D. (2011). Tissue distribution and gender-divergent expression of 78 cytochrome P450 mRNAs in mice. *Toxicological sciences*, *124*(2), 261-77. https://doi.org/10.1093/toxsci/kfr240

Rice, J. C., Spence, J. S., Megyesi, J., Goldblum, R. M., & Safirstein, R. L. (1999). Expression of the polymeric immunoglobulin receptor and excretion of secretory IgA in the postischemic kidney. *American Journal of Physiology-Renal Physiology*, *276*(5), F666-73. https://doi.org/10.1152/ajprenal.1999.276.5.F666

Robertson, L. T., Trevino-Villarreal, J. H., Mejia, P., Grondin, Y., Harputlugil, E., Hine, C., Vargas, D., Zheng, H., Ozaki, C. K., Kristal, B. S., & Simpson, S. J. (2015). Protein and calorie restriction contribute additively to protection from renal ischemia reperfusion injury partly via leptin reduction in male mice. *The Journal of nutrition*, *145*(8), 1717-27. https://doi.org/10.3945/jn.114.199380

Sandhi, J., Singh, J. P., Kaur, T., Ghuman, S. S., & Singh, A. P. (2014). Involvement of progesterone receptors in ascorbic acid–mediated protection against ischemia-reperfusion–induced acute kidney injury. *Journal of surgical research*, *187*(1), 278-88. https://doi.org/10.1016/j.jss.2013.10.025

Shu, X., Zhan, P. P., Sun, L. X., Yu, L., Liu, J., Sun, L. C., Yang, Z. H., Ran, Y. L., & Sun, Y. M. (2021). BCAT1 Activates PI3K/AKT/mTOR pathway and contributes to the angiogenesis and tumorigenicity of gastric cancer. *Frontiers in cell and developmental biology*, *2021*, 1345. https://doi.org/10.3389/fcell.2021.659260

Solati, Z., Edel, A. L., Shang, Y., O, K., & Ravandi, A. (2018). Oxidized phosphatidylcholines are produced in renal ischemia reperfusion injury. *PLoS One*, *13*(4), e0195172.

https://doi.org/10.1371/journal.pone.0195172

Tibshirani, R. (1996). Regression shrinkage and selection via the lasso. *Journal of the Royal Statistical Society: Series B (Methodological)*, *58*(1), 267-88. https://doi.org/10.1111/j.2517-6161.1996.tb02080.x

Wilkerson, M. D., & Hayes, D. N. (2010). ConsensusClusterPlus: a class discovery tool with confidence assessments and item tracking. *Bioinformatics*, *26*(12), 1572-3. https://doi.org/10.1093/bioinformatics/btq170

Wu, M. Y., Yiang, G. T., Liao, W. T., Tsai, A. P., Cheng, Y. L., Cheng, P. W., Li, C. Y., & Li, C. J. (2018). Current mechanistic concepts in ischemia and reperfusion injury. *Cellular Physiology and Biochemistry*, *46*(4), 1650-67. https://doi.org/10.1159/000489241

Yoshihara, K., Shahmoradgoli, M., Martínez, E., Vegesna, R., Kim, H., Torres-Garcia, W., Treviño, V., Shen, H., Laird, P. W., Levine, D. A., & Carter, S. L. (2013). Inferring tumour purity and stromal and immune cell admixture from expression data. *Nature communications*, *4*(1), 1-1. https://doi.org/10.1038/ncomms3612

You, R., Heyang, Z., Ma, Y., Xia, P., Zheng, H., Lin, J., Ji, P., & Chen, L. (2022). Identification of biomarkers, immune infiltration landscape, and treatment targets of ischemia–reperfusion acute kidney injury at an early stage by bioinformatics methods. *Hereditas*, *159*(1), 1-8. https://doi.org/10.1186/s41065-022-00236-x

Zeng, S., Feirt, N., Goldstein, M., Guarrera, J., Ippagunta, N., Ekong, U., Dun, H., Lu, Y., Qu, W., Schmidt, A. M., & Emond, J. C. (2004). Blockade of receptor for advanced glycation end product (RAGE) attenuates ischemia and reperfusion injury to the liver in mice. *Hepatology*, *39*(2), 422-32. https://doi.org/10.1002/hep.20045

Zhu, K., Zheng, T., Chen, X., & Wang, H. (2018). Bioinformatic analyses of renal ischaemia-reperfusion injury models: identification of key genes involved in the development of kidney disease. *Kidney and Blood Pressure Research*, *43*(6), 1898-907. https://doi.org/10.1159/000496001